Cell

Mechanism of Transcriptional Bursting in Bacteria

Shasha Chong,[1,5] Chongyi Chen,[1,2,5] Hao Ge,[3,4] and X. Sunney Xie[1,3,*]
[1]Department of Chemistry and Chemical Biology, Harvard University, Cambridge, MA 02138, USA
[2]Department of Molecular and Cellular Biology, Harvard University, Cambridge, MA 02138, USA
[3]Biodynamic Optical Imaging Center (BIOPIC), Peking University, Beijing 100871, China
[4]Beijing International Center for Mathematical Research (BICMR), Peking University, Beijing 100871, China
[5]Co-first author
*Correspondence: xie@chemistry.harvard.edu
http://dx.doi.org/10.1016/j.cell.2014.05.038

SUMMARY

Transcription of highly expressed genes has been shown to occur in stochastic bursts. But the origin of such ubiquitous phenomenon has not been understood. Here, we present the mechanism in bacteria. We developed a high-throughput, in vitro, single-molecule assay to follow transcription on individual DNA templates in real time. We showed that positive supercoiling buildup on a DNA segment by transcription slows down transcription elongation and eventually stops transcription initiation. Transcription can be resumed upon gyrase binding to the DNA segment. Furthermore, using single-cell mRNA counting fluorescence in situ hybridization (FISH), we found that duty cycles of transcriptional bursting depend on the intracellular gyrase concentration. Together, these findings prove that transcriptional bursting of highly expressed genes in bacteria is primarily caused by reversible gyrase dissociation from and rebinding to a DNA segment, changing the supercoiling level of the segment.

INTRODUCTION

Essential for all cell functions, transcription, the synthesis of mRNAs from DNA carried out by RNA polymerase (RNApol), is the first step in gene expression. Many recent experiments have shown the general phenomenon that transcription of highly expressed genes occurs in stochastic bursts in bacteria (Golding et al., 2005; So et al., 2011; Taniguchi et al., 2010; Zong et al., 2010) and eukaryotic cells (Suter et al., 2011). A major source of gene expression noise, transcriptional bursting results in cellular diversity of an isogenic population, possibly enhancing survival of the population in the face of environmental uncertainty (Kussell and Leibler, 2005; Thattai and van Oudenaarden, 2004; Wolf et al., 2005). Golding and coworkers directly observed transcriptional bursting in real time by using MS2 loops to monitor mRNA production in *E. coli* (Golding et al., 2005). Our group reported a high-throughput, single-molecule fluorescence in situ hybridization (FISH) assay to measure the cellular copy number distribution of a particular mRNA for a large population of isogenic *E. coli* cells (Taniguchi et al., 2010). When mRNAs are generated with a constant flux, one expects a Poisson distribution of mRNAs across the population. Bursting transcription would lead to non-Poissonian distributions. For all the highly expressed *E. coli* genes, we found that the distributions are not Poissonian, with the Fano factor (variance divided by the mean of a given distribution) larger than one. This indicates the ubiquity of transcriptional bursting in bacteria.

However, the origin of bacterial transcriptional bursting is still unknown. Its stochasticity implies it is a single-molecule behavior: there is only one copy of the gene in the cell. Its universality implies that it cannot be attributed to a specific gene or protein factor. Rather, it must originate from a fundamental and general mechanism pertinent to the chromosomal DNA structure and its influence on transcription regulation.

It has been shown that *E. coli* chromosomal DNA is segregated to ~400 topologically constrained loops with an average size of 10,000 base pairs (Hardy and Cozzarelli, 2005; Postow et al., 2004). Recent work discussed that *E. coli* nucleoid-associated proteins such as H-NS and Fis can cause formation of DNA loops based on both chromosome conformation capture and superresolution optical imaging experiments (Wang et al., 2011). Such chromosome structure provides us a clue to explain the transcriptional bursting phenomenon (Figure 1). In such a DNA loop, transcription generates positive supercoiling ahead of the RNApol and negative supercoiling behind the RNApol (Deng et al., 2004; Liu and Wang, 1987; Samul and Leng, 2007; Tsao et al., 1989; Wu et al., 1988). There exist two major topoisomerases in *E. coli* cells, gyrase and topoisomerase I (Topo I), which release positive and negative supercoiling, respectively (Drlica, 1992). It is known that negative supercoiling formed during transcription elongation is rapidly removed by Topo I (Cheng et al., 2003). This is necessary because accumulation of negative supercoiling could lead to the formation of detrimental R loops, an RNA-DNA hybrid (Drolet, 2006). The activity of gyrase, on the other hand, is not as sufficient to keep up with transcription (Guptasarma, 1996), leading to positive supercoiling accumulation on the DNA loops containing highly transcribed operons (El Hanafi and Bossi, 2000).

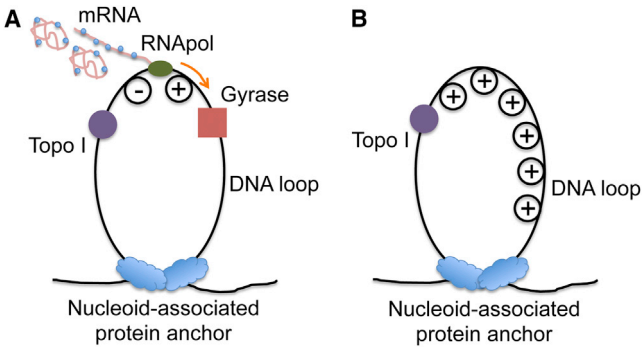

Figure 1. Transcription on Topologically Isolated Chromosomal DNA Loops

(A) Gyrase releases positive supercoiling generated by transcription on a DNA loop, and RNApol keeps transcribing the gene.

(B) In the absence of gyrase, active transcription on a DNA loop leads to positive supercoiling accumulation, which inhibits further transcription on the particular DNA loop.

It has been found that there are ~500 gyrase molecules per *E. coli* cell (Baker et al., 1987; Higgins et al., 1978; Liu and Wang, 1987), which happens to be roughly the number of topologically constrained DNA loops per chromosome. On average, there is one gyrase molecule per DNA loop. When a gyrase molecule reacts on the DNA loop, positive supercoiling is released, and RNApol can keep transcribing the gene ("on" state; Figure 1A). When the gyrase dissociates from the loop, positive supercoiling is built up by transcription, possibly slowing down transcription elongation and stopping transcription initiation ("off" state; Figure 1B).

In this study, through a series of in vitro single-molecule and live-cell experiments, we prove that transcriptional bursting of highly expressed genes in bacteria is primarily caused by gyrase dissociation from and reversible binding to a DNA segment or a chromosomal loop, which changes the supercoiling level of the DNA segment.

RESULTS

An In Vitro, Single-Molecule Assay Allows Real-Time Monitoring of Transcription on Individual DNA Templates

We developed an in vitro, single-molecule assay to monitor repetitive stochastic transcription events in real time on individual DNA templates with controlled supercoiling levels (Figure 2A). We used a nucleic acid stain, SYTO RNASelect (Life Technologies), which is nonfluorescent at 530 nm but becomes fluorescent upon binding to RNA (Figure 2B). It has been used to detect RNA in the presence of DNA (Kannemeier et al., 2007). An argon laser line at 488 nm was used to excite SYTO RNASelect in a total internal reflection fluorescence (TIRF) microscope. We collected fluorescence at 530 nm and recorded time-lapse movies with a charge-coupled device (CCD) camera. In the presence of the dye, a single nascent mRNA becomes visible, and its fluorescence intensity increases with the mRNA length. Therefore, we were able to track transcription elongation in real time as the nascent mRNA being produced on a surface-tethered DNA template. Transcription activities on up to hundreds of templates in one field of view can be monitored simultaneously.

As a control, we examined the effect of SYTO RNASelect on the activities of enzymes involved in our system, including T7 RNApol, *E. coli* RNApol, *E. coli* gyrase, and *E. coli* Topo I. None of them were found to be affected by the stain (Figures S1A–S1H available online). With sufficiently low laser power and the presence of a fresh oxygen scavenger system, photobleaching of the dye and photocleavage of nucleic acids were negligible (Figure S2).

In our single-molecule assay, DNA templates containing a promoter were tethered on the passivated surface of the flow cell through biotin-streptavidin linkage. After we flowed RNApol and nucleoside triphosphates (NTPs) into the flow cell, the fluorescence intensity of many spots in the field of view linearly ramped up due to transcription elongation, followed by abrupt disappearance upon transcription termination (Figure 2C). "Blinking" of fluorescence occurred when multiple transcripts were produced. As a control, no fluorescence intensity increase was observed under any of the following conditions: (1) no RNApol in the solution, (2) no NTPs in the solution, and (3) no promoter in the DNA template. Full-length transcripts (>12 kb) were generated as confirmed by RNA gel electrophoresis (Figures S1G–S1I).

By recording fluorescent movies, we were able to measure intensity versus time for a field of view containing hundreds of individual DNA templates, from which we could monitor how individual transcripts were generated (Figure 2D). This in vitro, single-molecule assay allows us to investigate the effects of supercoiling on transcription initiation and elongation in a clean and controlled system.

Positive Supercoiling Buildup by Transcription Slows Down Transcription Elongation

We examined the effect of positive supercoiling buildup on transcription elongation in vitro. We designed 12-kb-long linear DNA templates with T7 or *E. coli* promoter on the 5′ end and single or multiple biotinylated nucleotides on the 3′ end (Figure 3A).

When the DNA duplex is tethered to the surface with a single biotin-streptavidin linkage, we found the average T7 transcription elongation rate is 53.2 ± 3.4 nt/s (0.3 mM each NTP; 23°C), which is consistent with previously reported rates (Skinner et al., 2004). This result further proved that transcription was not affected by the SYTO RNASelect dye. In this case, supercoiling cannot accumulate because DNA can rotate around its single linkage to the surface.

On the other hand, DNA with multiple biotinylated nucleotides cannot rotate around its multiple linkages to the surface. Positive supercoiling would accumulate downstream of the elongation complex when spiral of the bulky complex around the DNA is hindered by the frictional drag on the complex. Interestingly, we found T7 transcription elongation was slowed down by 38% as positive supercoiling accumulated on the multiple-biotin DNA template (Figure 3B).

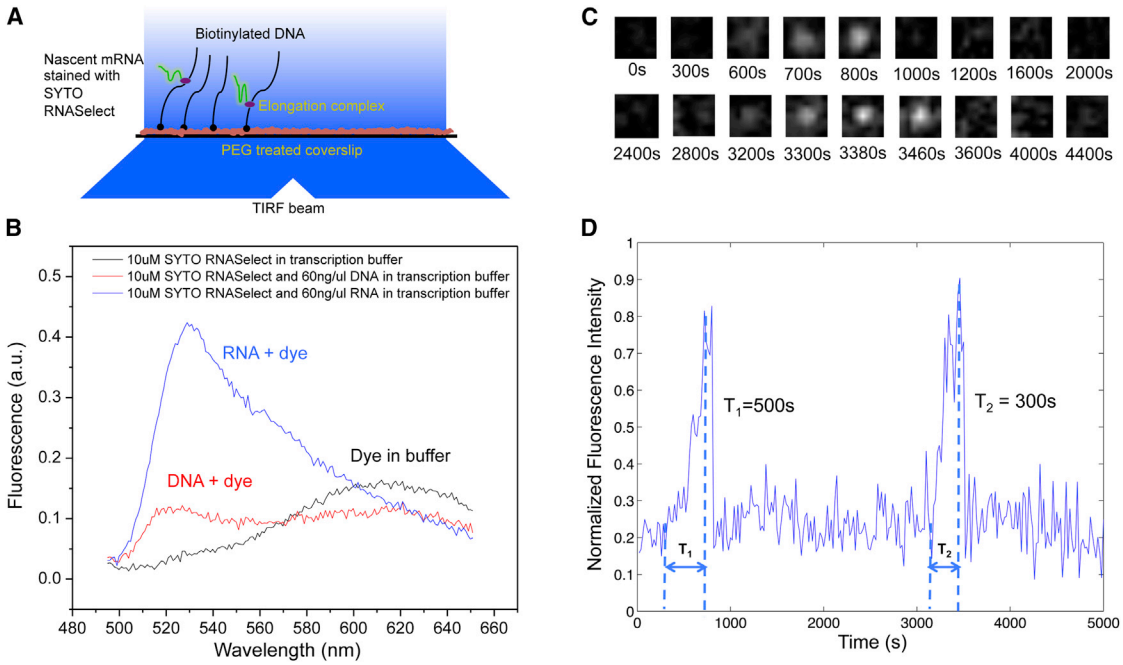

Figure 2. In Vitro, Single-Molecule Assay to Monitor Real-Time Transcription on Individual DNA Templates Using SYTO RNASelect Stain

(A) Schematic representation of the experimental arrangement (not drawn to scale). In the presence of 250 nM SYTO RNASelect, nascent RNAs are fluorescent under TIRF excitation at 488 nm. With an excitation power density of 0.22 W/cm^2 and an image acquisition time of 5 s, a transcript of 2,300 nucleotides yields a signal-to-noise ratio of 1.

(B) Fluorescence emission spectra of SYTO RNASelect solution under 488 nm excitation. The dye selectively stains RNA and emits fluorescence with a peak at 530 nm. In the absence of nucleic acids, the dye is not fluorescent at 530 nm. a.u., arbitrary units.

(C) Time-lapse images of 1.1 × 1.1 μm sub-field of view to monitor T7 transcription on one 12-kb-long template.

(D) Intensity-versus-time trajectory of the DNA template shown in (C). Full transcripts are produced repetitively on the template, with transcription elongation time T_1 = 500 s and T_2 = 300 s, respectively.

See also Figures S1 and S2.

There is a concern that supercoiling might arise from immobilization of the elongation complex to the surface. Special care was taken to minimize interactions of the elongation complex with the surface in our experiment. Besides, we note our result is consistent with the earlier in vitro report that the frictional drag on a sizable nascent transcript is enough to lead to DNA supercoiling (Tsao et al., 1989) even in aqueous solution and free of surface perturbation. Moreover, the measured elongation rate with the single linkage did not seem to be perturbed by the surface interaction with the elongation complex, if any.

Interestingly, the elongation rate on the multiple-biotin template was recovered when gyrase was added into the system. Figure 3C shows the elongation rate as a function of gyrase concentration, reaching the value of the single-biotin template at a saturating gyrase concentration. As a control, we found that gyrase did not affect the elongation rate on the single-biotin template (Figure 3C), indicating that gyrase play no other role than releasing positive supercoiling.

Similarly, with *E. coli* RNApol, we found positive supercoiling accumulation on the multiple-biotin template also slowed down transcription elongation by 47% (Figure 3D), which is consistent with a recent report based on mechanical manipulation (Ma et al., 2013).

Dissociation Constant of Gyrase-DNA Complex Is Determined from Gyrase Concentration Dependence of Transcription Elongation Rates

Gyrase-DNA binding can be described by two steps (Gore et al., 2006). First, DNA and gyrase form a complex with limited protein-DNA-binding interface, which is prone to rapid dissociation. Second, a chiral DNA wrap is formed around gyrase, which in the presence of ATP generates negative DNA supercoils. Here, we discuss the binding stability and kinetics of the DNA wrapping state, which are relevant to transcription dynamics.

By titrating the elongation rate on the multiple-biotin template with gyrase (Figure 3C), we determined the gyrase-DNA dissociation constant K_d from the gyrase concentration at which the increase of the T7 transcription elongation rate reaches half of its saturation value, that is $K_d \approx 100$ nM (Extended Experimental Procedures). This K_d is larger than previously reported 0.2∼0.5 nM (Higgins and Cozzarelli, 1982; Maxwell and Gellert, 1984), where specific gyrase-binding sequences were used (Morrison and Cozzarelli, 1981; Rau et al., 1987). Strong gyrase-binding sites comparable to these sequences are sparsely distributed on the *E. coli* chromosome with a frequency of only one per 100 kb (Snyder and Drlica, 1979). The *nuoB-N* DNA sequence (∼12 kb) we used in our in vitro assay better represents a chromosomal DNA loop (∼10 kb) that binds to gyrase

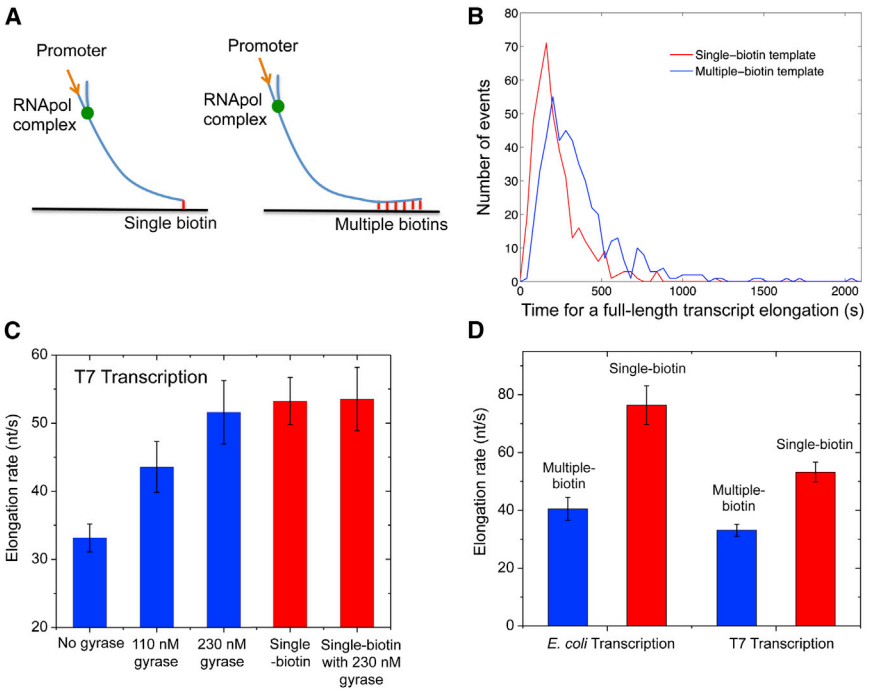

Figure 3. Supercoiling Dependence of Transcription Elongation Rate

(A) In vitro transcription template design containing a T7 or T7A1 promoter and a 12 kb transcribing sequence. The template is anchored to the flow cell surface via either a single or multiple biotin-streptavidin linkages.

(B) Histogram of T7 transcription elongation time on the templates anchored with single (red curve) or multiple biotin-streptavidin linkages (blue curve). The average elongation time for the multiple-biotin template is 60% longer.

(C) Titration of T7 transcription elongation rate (23°C) on the multiple-biotin template (the three bars on the left) with gyrase concentration. The elongation rate increases with the gyrase concentration till it gets as high as that on the single-biotin template (the fourth bar). The elongation rate on the single-biotin template does not change in the presence of a saturating concentration of gyrase (the bar on the right).

(D) *E. coli* transcription elongation rate (37°C) and T7 transcription elongation rate (23°C) on the multiple-biotin template are slower than on the single-biotin template. In (C) and (D), the elongation rates are averaged from over 300 transcripts under each condition. The error bars are bootstrapped confidence intervals (Efron and Tibshirani, 1993).

See also Figures S1 and S2.

at multiple weak binding sites (Franco and Drlica, 1988; Reece and Maxwell, 1991).

Positive Supercoiling Buildup by Transcription Essentially Stops Transcription Initiation

Next, we examined the effect of positive supercoiling on transcription initiation. In order to mimic topologically isolated DNA loops in the bacterial chromosome, we designed a circular template (Figure 4A) and tethered it to the surface with multiple biotin-streptavidin linkages. The circular template consists of a T7 or *E. coli* promoter, a 12-kb-long transcribing sequence, and a T7 or *E. coli* terminator. Due to the low circularization efficiency, a significant fraction of the purified DNAs remained to be linear, which are also tethered on the flow cell surface and transcribed. We picked the circular templates for analysis by staining the DNA molecules with SYTOX Orange and imaging them under flow after recording transcription movies (Figure S3).

For a single template under steady-state condition, transcription initiation rate is the number of initiation events over a fixed period of time (frequency of "spikes" in the intensity trajectory from a template; Figure S4A). According to the ergodic principle, the initiation rate is the sum of initiated events from a population of templates at a specific time point. We measured the total intensity of the circular templates, which is proportional to the initiation rate.

We examined the first steady-state condition, in which T7 transcription occurs on the circular templates in the absence of Topo I and gyrase. A bulky elongation complex generates positive supercoiling ahead of it and negative supercoiling behind it, which annihilate each other when the elongation complex dissociates from the template upon transcription termination (Figure 4A). We found the initiation rate was indeed constant over time because of repetitive annihilation of supercoiling (Figure 4B).

We then examined the second steady-state condition, in which T7 transcription occurs on the circular templates in the presence of both Topo I and gyrase (Figure 4C). Because both positive and negative supercoiling on the DNA template is continuously removed, the initiation rate remained constant over time under this condition (Figure 4D), which is the same as that in the first steady-state condition (Figures S4C and S4D).

We now examine how positive supercoiling buildup would hinder transcription initiation. After introduction of Topo I, negative supercoiling is rapidly removed, and positive supercoiling is expected to accumulate on the circular template as multiple transcripts are made (Figure 4E). Indeed, we observed the initiation rate decreased over time (Figure 4F). Interestingly, the final intensity has dropped to under 20% of its initial value, indicating that transcription initiation was essentially stopped by the buildup of positive supercoiling. This final state corresponds to the gene "off" state. We found that it takes approximately nine rounds of T7 transcription to build up sufficient positive supercoiling that inhibits transcription initiation on a single template in vitro (Figure S4B and Extended Experimental Procedures).

Similar to T7 transcription, we found transcription initiation rate of *E. coli* RNApol dropped to ~25% after approximately five transcripts were produced from a circular template of the same length (12 kb) in the presence of Topo I (Figures 4E, 4G, and S5; Extended Experimental Procedures). We note that fewer than five rounds of transcription might be sufficient to

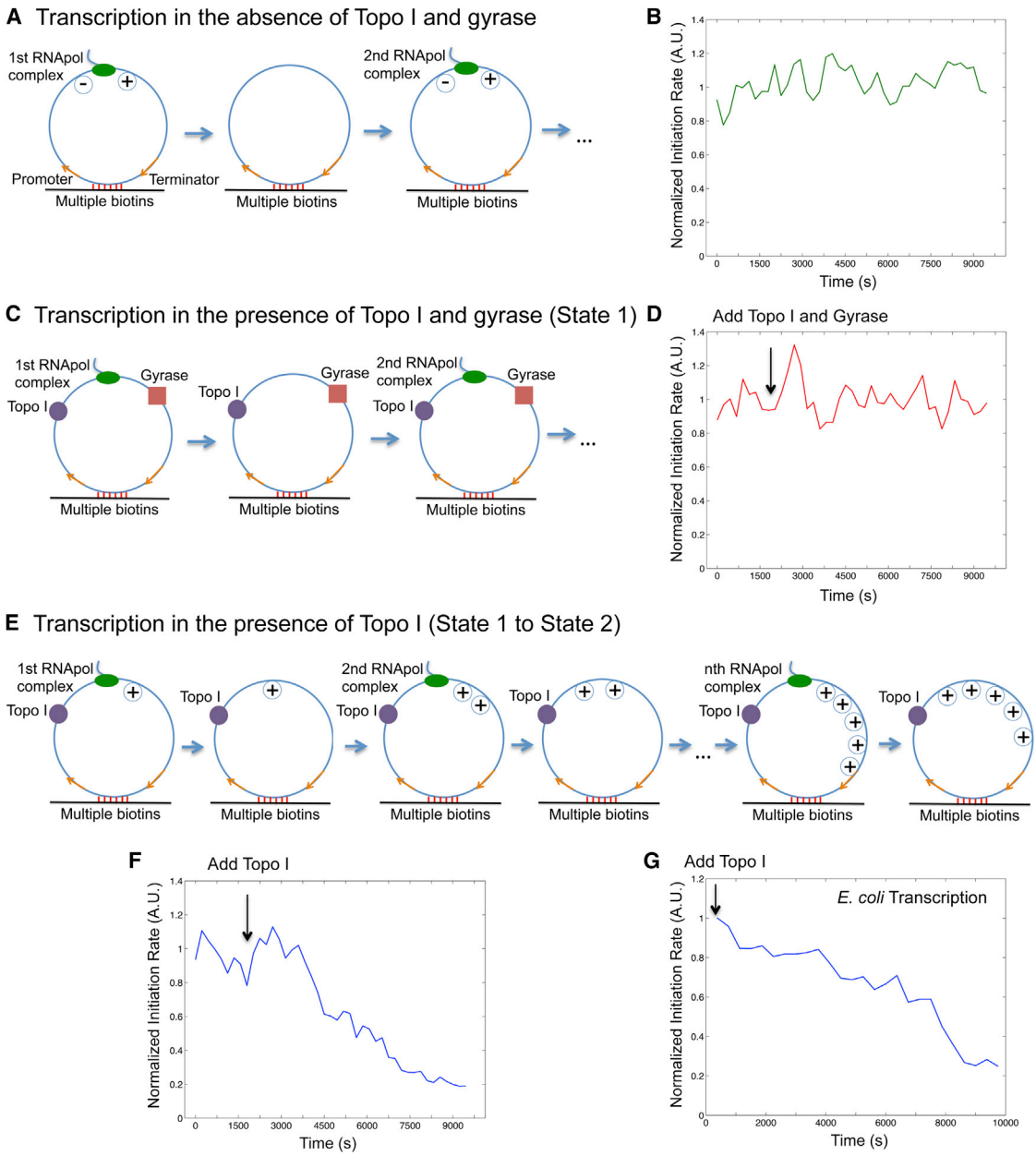

Figure 4. Supercoiling Dependence of Transcription Initiation Rate

(A) Schematic of transcription on a circular template in the absence of topoisomerases. Positive and negative supercoiling annihilate each other after RNApol completes transcription and dissociates from the template.

(B) Time dependence of T7 transcription initiation rate under the condition of (A).

(C) Schematic of transcription on the circular template in the presence of 41 nM Topo I and 0.1 μM gyrase (same as state 1 in Figure 7A).

(D) Time dependence of T7 transcription initiation rate under the condition of (C). The arrow shows the time when the topoisomerases were added into the system.

(E) Schematic of transcription on the circular template in the presence of 41 nM Topo I and absence of gyrase. Positive supercoiling is built up as transcripts are produced.

(F) Time dependence of T7 transcription initiation rate under the condition of (E). (B), (D), and (F) are the total intensity versus time from 160 circular templates under respective conditions normalized to the same fluorescence intensity.

(G) Time dependence of *E. coli* transcription initiation rate in the presence of 62 nM Topo I and absence of gyrase. This is the intensity averaged from 106 circular templates at each time point normalized to that from 209 linear templates (Extended Experimental Procedures).

See also Figures S1, S2, S3, S4, and S5.

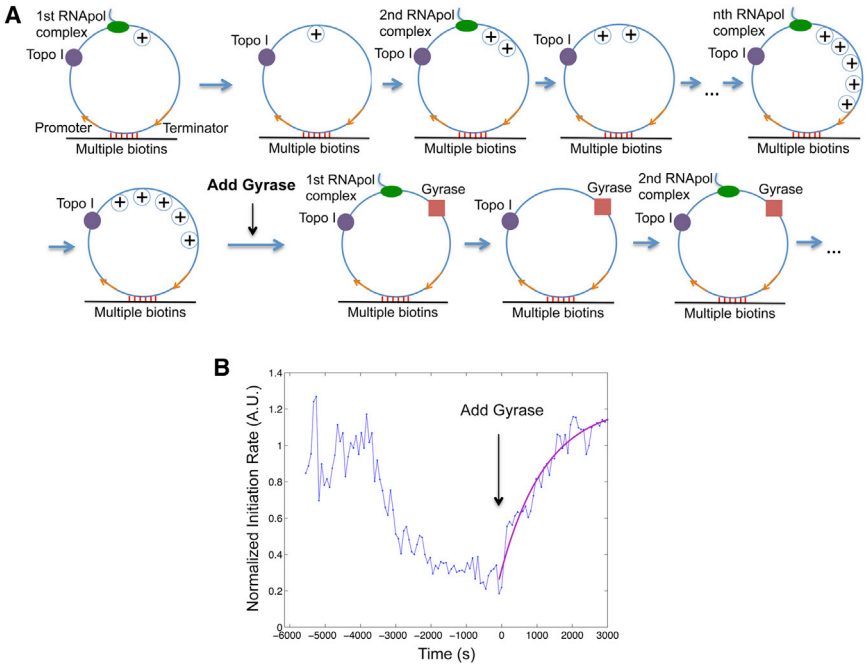

Figure 5. Transition from Gene Off to On State

(A) Schematic of transcription on the circular template first in the presence of 41 nM Topo I only (same as Figure 4E) and then both 41 nM Topo I and 0.1 μM gyrase (same as Figure 4C).

(B) Time dependence of T7 transcription initiation rate (blue) under the condition of (A). This is the intensity averaged from 160 circular templates at each time point normalized to that from 120 linear templates. Gyrase was added into the system at T = 0, when transcription initiation was essentially stopped by positive supercoiling accumulation. The trajectory after T = 0 is fitted with a single exponential function (magenta).

See also Figures S1, S2, and S3.

generate the same level of supercoiling in a live cell, where the environment is more viscous and the elongation complex is bulkier due to transcription-translation coupling (Lynch and Wang, 1993).

With regards to why supercoiling stops transcription initiation, earlier magnetic tweezer experiments have shown that DNA positive supercoiling leads to significantly slower and less stable formation of *E. coli* RNApol-promoter open complex (Revyakin et al., 2004). Therefore, we conclude that the observed inhibition of transcription initiation arises from hindered formation of RNApol-promoter open complex due to positive supercoiling accumulation.

Gyrase Binding to Positively Supercoiled DNA Restarts Transcription

We now prove that gyrase binding on the positively supercoiled DNA restarts transcription. We started with T7 transcription on the circular templates in the presence of Topo I, generating the gene off state (Figure 5). Upon addition of gyrase into the system, transcription initiation rate started to increase and reached a plateau at the initial value of the relaxed templates (Figure 5B), indicating that transcription initiation was fully recovered when positive supercoiling was released by gyrase.

The initiation rate versus time after the introduction of gyrase can be fitted well with a single exponential rise (Figure 5B), suggesting a single step is rate limiting for the transition. The rate constant is determined to be 0.78×10^{-3} s^{-1}, comparable to the pseudo-first-order gyrase-DNA binding rate constant $\sim 10^{-3}$ s^{-1}, which is the product between the bimolecular binding rate constant $k_{on} \approx 10^4$ M^{-1} s^{-1} under our salt concentration (Higgins and Cozzarelli, 1982) and the gyrase concentration used in our in vitro assay 0.1 μM. Such consistency suggests that gyrase binding to the DNA template is the rate-limiting step to restart transcription in vitro.

The K_d and k_{on} of gyrase-DNA binding determined in vitro allow us to estimate the time it takes gyrase to dissociate from and rebind to a specific chromosomal DNA loop in an *E. coli* cell. Because there are comparable numbers of gyrase molecules and chromosomal DNA loops per *E. coli* cell, many gyrase molecules are trapped on DNA loops. According to K_d, the intracellular concentration of unbound gyrase [G] is ~0.3 μM (Extended Experimental Procedures). Because k_{on} of gyrase-DNA binding is $\sim 10^4$ M^{-1} s^{-1} as determined in vitro, the in vivo pseudo-first-order rate constant for gyrase-DNA binding $k_{on} \cdot [G]$ is $\sim 3 \times 10^{-3}$ s^{-1}. Therefore, the average gyrase rebinding time is $1/(k_{on} \cdot [G]) \approx 6$ min. Because the dissociation rate constant of gyrase-DNA complex is $k_{off} = K_d \cdot k_{on} \approx 10^{-3}$ s^{-1}, the average gyrase dissociation time is $1/k_{off} \approx 17$ min. The gyrase rebinding and dissociation time is in the same order of magnitude with the off and on periods of transcriptional bursting observed in live *E. coli* cells (Golding et al., 2005).

In summary, the in vitro experiments demonstrated that DNA positive supercoiling generated by transcription slows down both transcription initiation and elongation and eventually stops initiation. Inhibited transcription initiation and elongation can be recovered upon gyrase binding to DNA. Therefore, accumulation and removal of positive supercoiling of a chromosomal DNA loop containing a highly expressed gene can switch the gene off and on. Next, we performed live-cell experiments to further support this mechanism.

Live-Cell Experiments Confirm that Positive Supercoiling Buildup Slows Down Transcription Elongation

We examined whether chromosomal supercoiling level affects transcription elongation in live *E. coli* cells. Using quantitative RT-PCR, we measured the steady-state abundance of different segments of fully induced *lac* operon mRNA under gyrase

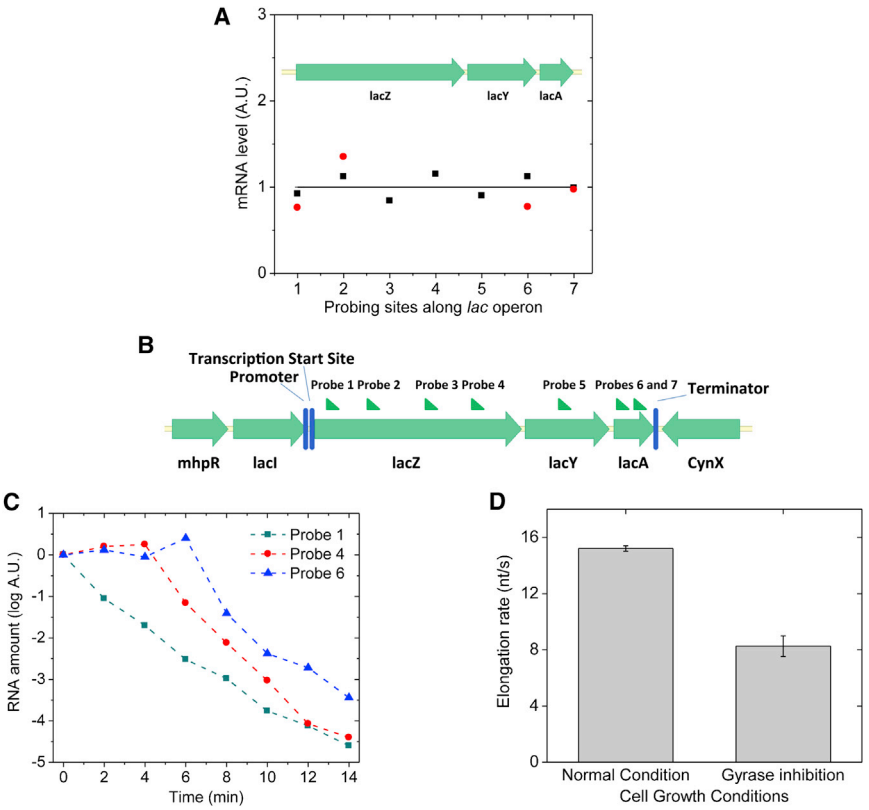

Figure 6. Transcription Processivity and Elongation Rate upon Gyrase Inhibition in Live *E. coli* Cells

(A) Quantitative RT-PCR measurement of the abundance of different parts of *lac* operon mRNA under fully induced condition. x axis: the position of probing sites along *lac* operon; y axis: mRNA abundance. Black squares: gyrase partial inhibition by 50 ng/μl novobiocin; red dots: gyrase complete inhibition by 10 ng/μl norfloxacin. The result indicates nonstop transcription elongation upon positive supercoiling buildup on the DNA. The abundance of each mRNA part is normalized to its abundance under wild-type condition, which is plotted as the flat curve.

(B) Seven sites on *lac* operon mRNA that were probed in the measurement of transcription elongation rate.

(C) Five hundred nanograms per microliter rifampicin was added into the cell culture at time zero to stop transcription initiation, but not elongation. The abundance of different positions on the *lac* operon mRNA was probed by quantitative RT-PCR at multiple time points.

(D) Transcription elongation rate decreased upon gyrase inhibition by 10 ng/μl norfloxacin in live *E. coli* cells. The error bars are SDs of the elongation rates obtained by repeating the measurements (n = 3) under each condition.

See also Figure S6.

inhibition by novobiocin or norfloxacin. No difference in the abundance was observed throughout the transcript (Figure 6A). This result suggests that the elongation complex does not stop or dissociate from the DNA template in the middle of one round of transcription more often when the DNA template is more positively supercoiled. We note that an early in vitro experiment found that stable norfloxacin-gyrase-DNA complex could form at a strong gyrase-binding site and block transcription elongation (Willmott et al., 1994). This effect was not observed in our live-cell assay, likely due to a low intracellular norfloxacin concentration and the lack of strong gyrase-binding sites in the probed region.

Next, we measured transcription elongation rate in live *E. coli* cells using transcription initiation inhibitor rifampicin (Epshtein and Nudler, 2003) and quantitative RT-PCR (H. Chen, K. Shiroguchi, H.G., and X.S.X., unpublished data). We added rifampicin to the cell culture at time zero and measured the mRNA abundance in multiple regions (Figure 6B) along the transcript at multiple time points afterward. Whereas the mRNA abundance at the 5′ end decreased immediately upon the addition of rifampicin, the mRNA abundance downstream started to decrease after a time delay (Figure 6C). The distance between the two probes on the transcript divided by the time delay was the elongation rate. Gyrase inhibition was achieved by norfloxacin treatment where most cells were viable through the 14-min-long rifampicin assay (Figure S6A). We found that the elongation rate of fully induced *lac* operon decreased by 46% upon gyrase inhibition (Figure 6D), similar to the result previously reported by Higgins group on *Salmonella enterica* (Rovinskiy et al., 2012).

A Two-State Model Describes Transcriptional Bursting

Transcriptional bursting has been described with a two-state model, but the origin of the two states was not understood (Golding et al., 2005; Munsky et al., 2012; So et al., 2011). We now understand the mechanism of bacterial transcriptional bursting (Figure 7A): the gene stochastically switches between on and off states due to release and accumulation of positive supercoiling. The on state (state 1) generates mRNAs with an average transcription rate k_1, and the mRNAs degrade with rate constant γ. The off state (state 2) does not generate any mRNA. The interconversion rate constants between the two states are α and β. α is the gene on-to-off transition rate constant due to gyrase dissociation from the DNA loop and positive supercoiling accumulation. For simplicity, we assume positive supercoiling accumulation is fast and gyrase dissociation is rate limiting. β corresponds to the pseudo-first-order rate constant of gyrase-DNA binding, which is also rate limiting in the gene off-to-on transition and proportional to the effective intracellular gyrase concentration. The lower the effective gyrase concentration is, the longer the gene stays in the off state and the smaller the on/off duty cycle ratio (β/α), which should result in a higher extent of bursting reflected by a larger Fano factor and a larger fraction of cells that contain zero copy of mRNA at a given time point.

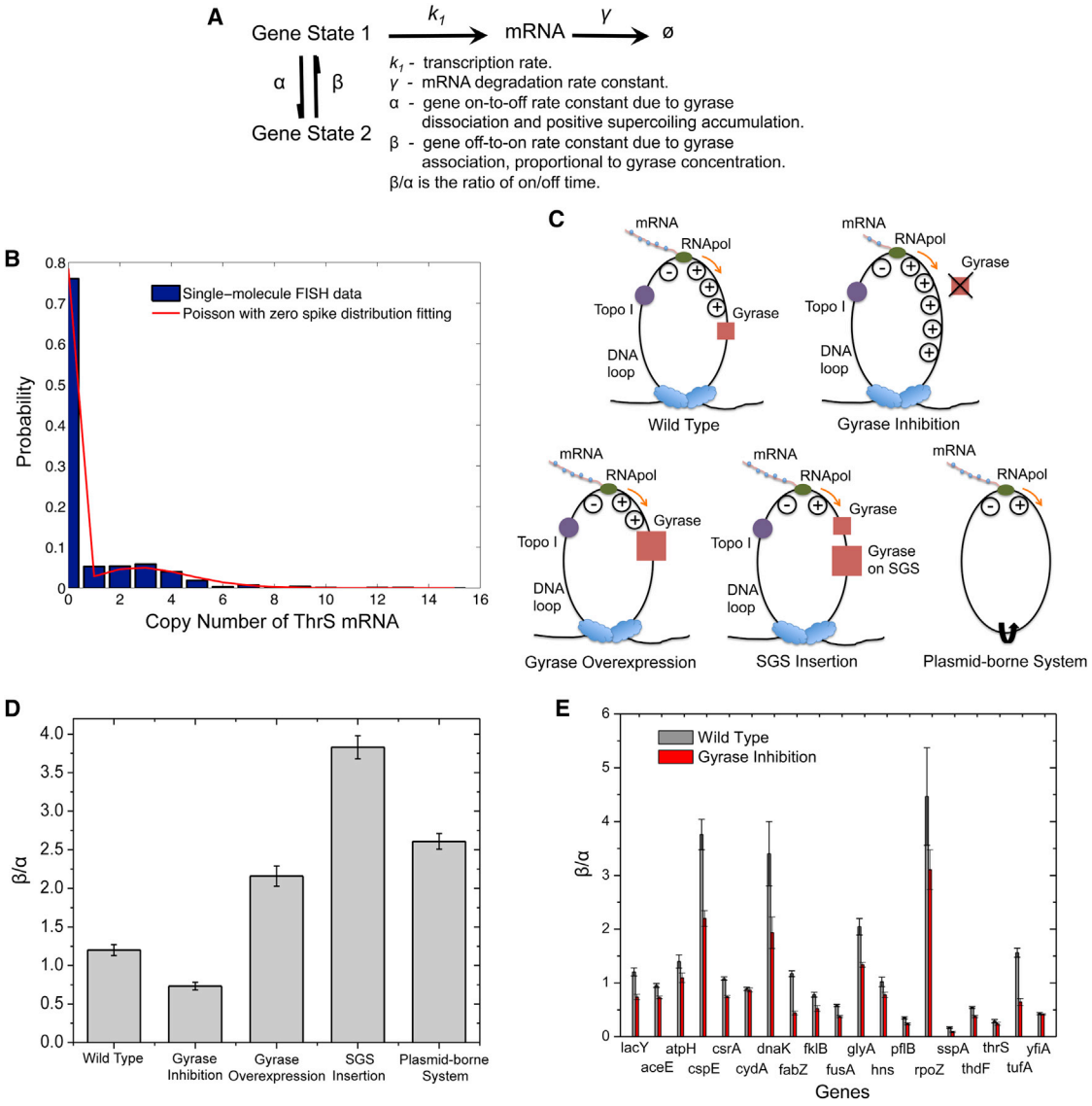

Figure 7. Dependence of On/Off Duty Cycle Ratio, β/α, on Effective Intracellular Gyrase Concentration

(A) Kinetic scheme of the two-state model with relevant rate constants.

(B) Fitting of cellular ThrS mRNA copy number distribution with Poisson with zero spike distribution.

(C) Schematics of interactions between effective gyrase concentration and DNA supercoiling generated by transcription under different conditions. Upon gyrase inhibition, positive supercoiling accumulates on the chromosomal DNA loop to a higher extent than wild-type. Gyrase overexpression or SGS insertion is the opposite. In a plasmid-borne expression module, positive and negative supercoiling annihilate each other due to the lack of topological barriers.

(D) β/α of fully induced *lac* operon decreases upon gyrase partial inhibition by 50 ng/μl novobiocin treatment and increases upon gyrase overexpression, SGS insertion, and in a plasmid-borne system.

(E) β/α of fully induced *lac* operon and other 18 highly transcribed *E. coli* genes. β/α of all the 19 genes decrease upon gyrase partial inhibition by 50 ng/μl novobiocin treatment. In (D) and (E), the error bars are bootstrapped confidence intervals.

See also Figures S6, S7, and Table S1.

Transcription bursts of highly transcribed genes are reflected by the non-Poissonian mRNA copy number distribution. Under the condition that α and β are significantly smaller than k_1 and γ as previously observed (Golding et al., 2005), the steady-state mRNA copy number distribution for a population of cells is bimodal (Munsky et al., 2012) and can be approximated with a "Poisson with zero spike" distribution (Equation 1). Based on the two-state model, the Fano factor (F) can be derived as Equation 2 (Extended Experimental Procedures).

$$p(0) = \frac{\beta}{\alpha+\beta} e^{-\frac{k_1}{\gamma}} + \frac{\alpha}{\alpha+\beta}$$
$$p(n) = \frac{\beta}{\alpha+\beta} e^{-\frac{k_1}{\gamma}} \frac{\left(\frac{k_1}{\gamma}\right)^n}{n!}, n \geq 1. \quad \text{(Equation 1)}$$

$$F = 1 + \frac{\alpha k_1}{(\alpha+\beta)\gamma}. \quad \text{(Equation 2)}$$

We note these results hold only under the condition that gyrase dissociation and rebinding are rate limiting, longer than the time scales of positive supercoiling accumulation and release. Although this is a simplified model, it captures the origin of transcriptional bursting, i.e., gyrase dissociation, and establishes the gyrase concentration dependence of β, which can now be subject to in vivo experimental tests.

The Dependence of Transcriptional Bursting on Effective Gyrase Concentration Revealed by Single-Molecule mRNA FISH Assay

We now experimentally verify this model by measuring the steady-state mRNA copy number distribution in a population of isogenic *E. coli* cells under gyrase inhibition and overexpression conditions. We performed mRNA FISH assay with single-molecule sensitivity, using a single Atto 594-labeled 20-oligomer nucleotide probing the *yfp* sequence in an *E. coli* strain with the target gene fused to *yfp* sequence endogenously. By measuring the intensity of each fluorescent spot and counting the number of spots per cell, we determined cellular mRNA copy number for thousands of *E. coli* cells. The efficiency of our single-molecule mRNA FISH assay is ~90% (Taniguchi et al., 2010).

We measured the cellular mRNA copy number distribution of the fully induced *lac* operon and 18 highly transcribed genes from the YFP library that our group has constructed (Taniguchi et al., 2010). Partial gyrase inhibition was achieved by novobiocin treatment at low concentration without affecting normal bacterial growth and morphology (Figure S6B). We found that the cellular mRNA copy number distribution can be fitted well by the Poisson with zero spike distribution for the 19 genes with excellent coefficients of determination (Figure 7B; Table S1). The fitting allows estimation of the on/off duty cycle ratio of transcriptional bursting (β/α), with an error bar obtained by the bootstrapping method (Efron and Tibshirani, 1993).

For fully induced *lac* operon, β/α was 1.20 for wild-type, decreased to 0.73 upon gyrase inhibition, increased to 2.16 upon gyrase overexpression, and increased to 3.83 when a strong gyrase site (SGS) was inserted next to the *lac* operon (Figures 7C and 7D). This result indicates that transcriptional bursting is sensitively dependent on the availability of gyrase to remove positive supercoiling accumulated during active transcription.

If *lac* operon is on a plasmid that lacks topological constraint, positive and negative supercoiling generated by transcription could diffuse along the circular DNA in opposite directions and annihilate each other (Figure 7C). As a critical control, a plasmid-borne system in *E. coli* indeed showed an even higher β/α than that of gyrase overexpression (Figure 7D).

One would expect β/α to be infinitely large if the gene is always on in the complete absence of positive supercoiling accumulation. Yet it was not the case for the plasmid-borne system because there could be weak and transient topological barriers on the plasmid DNA due to transient protein binding (Leng et al., 2011). To confirm this point, we performed control experiments on the same plasmid-borne system under gyrase inhibition and overexpression conditions. We found that β/α changed in the same direction as the chromosomal gene but to a smaller extent. Under the same conditions, β/α of the plasmid-borne system was always higher than the chromosomal counterpart, because the plasmid has much lower topological barriers and thus more efficient removal of positive supercoiling during active transcription (Figure S6C).

Intriguingly, similar to the scenario of fully induced *lac* operon, all the other 18 genes showed a decreased β/α (Figure 7E) upon gyrase inhibition. In addition, most of the genes showed an increased Fano factor (Figure S7A) and an increased fraction of cells containing zero copy of mRNA (Figure S7B) upon gyrase inhibition. These findings are consistent with the prediction based on our model and demonstrate the ubiquitous effect of gyrase concentration on transcriptional bursting.

DISCUSSION

Mechanism of Transcriptional Bursting under Induced Condition Revealed

Pertinent to the fact that there is only one (or two) copy of the gene in a cell, gene expression is stochastic. In recent years, stochastic gene expression has stimulated wide interest (Blake et al., 2003; Elowitz and Leibler, 2000; Elowitz et al., 2002; Ozbudak et al., 2002; Pedraza and Paulsson, 2008). Such stochasticity, or noise, causes phenotypic variability among genetically identical cells and organisms despite identical histories of environmental exposure (Choi et al., 2008; Maamar et al., 2007) and arises from the fact that DNA, mRNA, and gene regulatory proteins can be present and active at only a few copies per cell. Due to the small copy numbers and the fact that stochastic gene expression cannot be synchronized among different cells, quantitative studies of gene expression at the single-cell level necessitate single-molecule sensitivity for mRNA and protein detection.

The stochastic gene expression dynamics of repressed genes have already been well studied and understood to date (Li and Xie, 2011). For highly expressed genes in both prokaryotic and eukaryotic organisms, bursting transcription has been demonstrated by a number of techniques, including single-molecule FISH assay that counts cellular mRNA copy number (Raj et al., 2006, 2010; Taniguchi et al., 2010; Zong et al., 2010), MS2 or PP7 technique that visualizes single mRNA production in real time (Chubb et al., 2006; Golding et al., 2005; Hocine et al., 2013; Larson et al., 2011; Lionnet et al., 2011; Muramoto et al., 2012), and fluorescent protein (Singh et al., 2010) or luciferase (Suter et al., 2011) as gene expression reporter in live cells. Nevertheless, the mechanism of this ubiquitous phenomenon under induced condition is not understood.

We note that the transcriptional bursting phenomenon studied in this paper is different from transcriptional pausing in prokaryotic and eukaryotic cells (Core et al., 2008; Landick, 2006;

Weixlbaumer et al., 2013), which has been studied by recent single-molecule manipulation (Davenport et al., 2000; Herbert et al., 2006; Hodges et al., 2009; Ma et al., 2013; Shundrovsky et al., 2004) and RNA-sequencing experiments (Churchman and Weissman, 2011; Core et al., 2008). Whereas pausing describes intermittent elongation of a transcript, bursting describes discontinuous production of many transcripts over a much longer time scale and involves inhibition of both transcription initiation and elongation.

We have revealed the origin of stochastic transcriptional bursts in bacteria under induced conditions by conducting a series of in vitro and live-cell experiments and demonstrated that reversible switching between different chromosomal supercoiling levels via gyrase dissociation from and rebinding to a DNA loop gives rise to bursting transcription. We note this is a fundamental mechanism pertinent to the chromosome structure and should be applicable to all the highly expressed genes in prokaryotic cells and even eukaryotic cells. However, the situation of eukaryotic cells is more complex than that of bacteria due to more complicated transcription regulation and the existence of nucleosomes (Raser and O'Shea, 2004).

A Role of DNA Supercoiling in Gene Expression Regulation

The interaction between DNA supercoiling and gene expression in bacteria has been investigated for decades. Our knowledge comes primarily from ensemble studies on the relationship between the global DNA supercoiling level and the gene expression level. On one hand, bacterial DNA supercoiling level affects the expression of a few *E. coli* genes called supercoiling-sensitive genes (Peter et al., 2004) as well as transcription elongation rate (Rovinskiy et al., 2012) due to a combined effect of torsional and bending stress sustained by the supercoiled DNA at the transcription site (Lionberger and Meyhöfer, 2010; ten Heggeler-Bordier et al., 1992). On the other hand, local DNA supercoiling level is generated by transcription, according to the "twin-domain model" developed by Wang and Liu groups in late 1980s (Deng et al., 2005; Leng et al., 2011; Lim et al., 2003; Liu and Wang, 1987; Samul and Leng, 2007; Tsao et al., 1989; Wu et al., 1988). Here, we report a role of DNA supercoiling in gene expression regulation that can only be revealed by single-molecule and single-cell approaches: transient DNA supercoiling generated locally during active transcription gives rise to transcriptional bursting, which is a major source of gene expression noise that causes cell-to-cell variability in an isogenic population. Although earlier work proposed DNA supercoiling can be involved in bursting transcription (Mitarai et al., 2008; So et al., 2011), we have experimentally proved that supercoiling dynamics is the primary origin of transcriptional bursting.

In Vitro, Single-Molecule Transcription Assay

In order to investigate the effect of positive supercoiling buildup on transcription elongation and initiation in a clean and controlled fashion, we developed an in vitro, single-molecule assay that could monitor real-time transcription on individual DNA templates. We note our assay is different from other existing in vitro transcription assays using single-molecule manipulation (Abbondanzieri et al., 2005; Bai et al., 2006; Billingsley et al., 2012; Bustamante et al., 2011; Herbert et al., 2008) or single-molecule fluorescence imaging (Chakraborty et al., 2012; Friedman and Gelles, 2012; Kapanidis et al., 2006; Revyakin et al., 2012; Tang et al., 2009; Zhang et al., 2014). Our assay uses RNA staining so that the elongation process on templates with any sequence can be easily monitored for multiple rounds of transcription on each template. This is a high-throughput measurement because hundreds of templates in one field of view can be monitored simultaneously. The assay will be generally useful for studying other questions in transcription, such as pausing and termination kinetics.

Other Possible Mechanisms of Transcriptional Bursting

The current report proves that stochastic changes of supercoiling level in DNA segments due to gyrase dissociation and rebinding is a main mechanism that gives rise to bursting transcription of highly expressed genes in bacteria. However, we note there could be other possible causes of bacterial transcriptional bursting, such as the change of chromosomal looping structure due to the dissociation and rebinding of nucleoid-associated proteins, as well as facilitated transcription reinitiation due to dynamical gene looping, where an operon DNA places its promoter and terminator in spatial proximity (Hebenstreit, 2013). Although they might cause transcription rate fluctuations in addition to the supercoiling effect that we observed, none of these alternative mechanisms have been experimentally proved to switch genes on and off.

EXPERIMENTAL PROCEDURES

In Vitro Single-Molecule Transcription Assay

To measure transcription elongation rates, T7 RNApol (New England Biolabs) or *E. coli* RNApol (Epicentre), NTPs, 250 nM SYTO RNASelect, and an oxygen scavenger system were added to transcription buffer. After infusing the mixture into the flow cell containing immobilized DNA templates, a fluorescent movie was recorded under 488 nm laser excitation at 0.22 W/cm^2. Images were taken every 20 s for 60–80 min, and the acquisition time of each image was 5 s.

To measure transcription initiation rates, the reaction mixture was the same as that for elongation rate measurements except that higher concentrations of RNApol and NTPs were used. The excitation power density was 0.15 W/cm^2. Images were taken every 75 s with 5 s of image acquisition time.

DNA Staining Assay

In order to locate the linear and circular templates in the field of view, 100 nM SYTOX Orange (Life Technologies) in 50 mM Tris-HCl buffer (pH 8.0) was used to stain the immobilized DNAs after transcription movies were recorded. Fluorescent movies were recorded under 532 nm laser excitation with a power density above 4 W/cm^2. The image acquisition time was 0.3 s. The imaging buffer was kept flowing at 8 ml/hr by a syringe pump (PhD 2000; Harvard Apparatus) during the movie recording.

Single-Molecule mRNA FISH Assay

The BW25993 *E. coli* cells were grown in M9 medium with 0.4% glycerol, amino acids, and vitamins, together with antibiotics and saturating amount of isopropyl β-D-thiogalactopyranoside (IPTG) if necessary. The cells were subsequently inoculated 1:500 into the same medium and incubated for ~7 hr at 37°C with 250 rpm shaking till optical density 600 nm (OD_{600nm}) reached 0.2~0.3. Fifty nanograms per microliter novobiocin (Sigma) was added into the medium and incubated for another 2 hr before harvest. Two hours was long enough (several cell cycles) to allow all the cells to enter steady state and thus minimized potential cell-to-cell variation due to different transition kinetics in response to the drug treatment.

The YFP library strains were grown in Luria broth (LB) medium with chloramphenicol at 30°C. The cells were subsequently inoculated 1:400 into M9 medium with 0.4% glucose, amino acids, and vitamins and incubated for 11 hr at 30°C with 250 rpm shaking till OD_{600nm} reached 0.2∼0.3. Fifty nanograms per microliter novobiocin was added and incubated for another 2 hr before harvest.

Single-molecule mRNA FISH assay was performed as previously described (Taniguchi et al., 2010) using Venus495r mRNA FISH probe covalently linked to a dye molecule Atto 594 (Sigma-Aldrich). The images were taken under epi-illumination by a fiber laser at 580 nm and phase contrast illumination by a halogen lamp.

SUPPLEMENTAL INFORMATION

Supplemental Information includes Extended Experimental Procedures, seven figures, and one table and can be found with this article online at http://dx.doi.org/10.1016/j.cell.2014.05.038.

AUTHOR CONTRIBUTIONS

X.S.X. conceived the project and supervised the experiments. S.C. developed the in vitro, single-molecule transcription assay. S.C. performed the in vitro imaging experiments, data analysis, and biophysical calculations based on the in vitro data. S.C. and C.C. performed the control of the enzyme activities in the in vitro, single-molecule transcription assay. C.C. performed the single-molecule mRNA FISH assay, data analysis, and live-cell experiments based on quantitative RT-PCR. C.C. made the DNA constructs for the in vitro, single-molecule assay and the FISH assay. H.G. built the mathematical model. H.G., C.C., and S.C fitted the model to the single-molecule FISH data. S.C., C.C., and X.S.X. designed the experiments and wrote the manuscript.

ACKNOWLEDGMENTS

We thank Xiaowei Zhuang for the collaboration on bacterial chromosomal structure study, which prompted us to conduct the current study; N. Patrick Higgins for providing the plasmid containing strong gyrase site sequence; Gene-Wei Li for development of FISH protocol; Minbiao Ji for help with microscope construction; Rahul Roy for advice on data analysis; and James Wang, Long Cai, Gene-Wei Li, and Paul Choi for critical reading of the manuscript. This work was supported by NIH Pioneer Award (1DP1OD000277; to X.S.X.), NIH grant TR01 (5R01GM096450-02; to X.S.X.), National Science Foundation of China (21373021; to H.G.), and the Foundation for the Author of National Excellent Doctoral Dissertation of China (201119; to H.G.).

Received: September 25, 2013
Revised: March 17, 2014
Accepted: May 8, 2014
Published: July 17, 2014

REFERENCES

Abbondanzieri, E.A., Greenleaf, W.J., Shaevitz, J.W., Landick, R., and Block, S.M. (2005). Direct observation of base-pair stepping by RNA polymerase. Nature *438*, 460–465.

Bai, L., Santangelo, T.J., and Wang, M.D. (2006). Single-molecule analysis of RNA polymerase transcription. Annu. Rev. Biophys. Biomol. Struct. *35*, 343–360.

Baker, T.A., Funnell, B.E., and Kornberg, A. (1987). Helicase action of dnaB protein during replication from the Escherichia coli chromosomal origin in vitro. J. Biol. Chem. *262*, 6877–6885.

Billingsley, D.J., Bonass, W.A., Crampton, N., Kirkham, J., and Thomson, N.H. (2012). Single-molecule studies of DNA transcription using atomic force microscopy. Phys. Biol. *9*, 021001.

Blake, W.J., KAErn, M., Cantor, C.R., and Collins, J.J. (2003). Noise in eukaryotic gene expression. Nature *422*, 633–637.

Efron, B., and Tibshirani, R.J. (1993). An Introduction to the Bootstrap (New York: Chapman & Hall).

Bustamante, C., Cheng, W., and Mejia, Y.X. (2011). Revisiting the central dogma one molecule at a time. Cell *144*, 480–497.

Chakraborty, A., Wang, D., Ebright, Y.W., Korlann, Y., Kortkhonjia, E., Kim, T., Chowdhury, S., Wigneshweraraj, S., Irschik, H., Jansen, R., et al. (2012). Opening and closing of the bacterial RNA polymerase clamp. Science *337*, 591–595.

Cheng, B., Zhu, C.X., Ji, C., Ahumada, A., and Tse-Dinh, Y.C. (2003). Direct interaction between Escherichia coli RNA polymerase and the zinc ribbon domains of DNA topoisomerase I. J. Biol. Chem. *278*, 30705–30710.

Choi, P.J., Cai, L., Frieda, K., and Xie, X.S. (2008). A stochastic single-molecule event triggers phenotype switching of a bacterial cell. Science *322*, 442–446.

Chubb, J.R., Trcek, T., Shenoy, S.M., and Singer, R.H. (2006). Transcriptional pulsing of a developmental gene. Curr. Biol. *16*, 1018–1025.

Churchman, L.S., and Weissman, J.S. (2011). Nascent transcript sequencing visualizes transcription at nucleotide resolution. Nature *469*, 368–373.

Core, L.J., Waterfall, J.J., and Lis, J.T. (2008). Nascent RNA sequencing reveals widespread pausing and divergent initiation at human promoters. Science *322*, 1845–1848.

Davenport, R.J., Wuite, G.J., Landick, R., and Bustamante, C. (2000). Single-molecule study of transcriptional pausing and arrest by E. coli RNA polymerase. Science *287*, 2497–2500.

Deng, S., Stein, R.A., and Higgins, N.P. (2004). Transcription-induced barriers to supercoil diffusion in the Salmonella typhimurium chromosome. Proc. Natl. Acad. Sci. USA *101*, 3398–3403.

Deng, S., Stein, R.A., and Higgins, N.P. (2005). Organization of supercoil domains and their reorganization by transcription. Mol. Microbiol. *57*, 1511–1521.

Drlica, K. (1992). Control of bacterial DNA supercoiling. Mol. Microbiol. *6*, 425–433.

Drolet, M. (2006). Growth inhibition mediated by excess negative supercoiling: the interplay between transcription elongation, R-loop formation and DNA topology. Mol. Microbiol. *59*, 723–730.

El Hanafi, D., and Bossi, L. (2000). Activation and silencing of leu-500 promoter by transcription-induced DNA supercoiling in the Salmonella chromosome. Mol. Microbiol. *37*, 583–594.

Elowitz, M.B., and Leibler, S. (2000). A synthetic oscillatory network of transcriptional regulators. Nature *403*, 335–338.

Elowitz, M.B., Levine, A.J., Siggia, E.D., and Swain, P.S. (2002). Stochastic gene expression in a single cell. Science *297*, 1183–1186.

Epshtein, V., and Nudler, E. (2003). Cooperation between RNA polymerase molecules in transcription elongation. Science *300*, 801–805.

Franco, R.J., and Drlica, K. (1988). DNA gyrase on the bacterial chromosome. Oxolinic acid-induced DNA cleavage in the dnaA-gyrB region. J. Mol. Biol. *201*, 229–233.

Friedman, L.J., and Gelles, J. (2012). Mechanism of transcription initiation at an activator-dependent promoter defined by single-molecule observation. Cell *148*, 679–689.

Golding, I., Paulsson, J., Zawilski, S.M., and Cox, E.C. (2005). Real-time kinetics of gene activity in individual bacteria. Cell *123*, 1025–1036.

Gore, J., Bryant, Z., Stone, M.D., Nöllmann, M., Cozzarelli, N.R., and Bustamante, C. (2006). Mechanochemical analysis of DNA gyrase using rotor bead tracking. Nature *439*, 100–104.

Guptasarma, P. (1996). Cooperative relaxation of supercoils and periodic transcriptional initiation within polymerase batteries. BioEssays *18*, 325–332.

Hardy, C.D., and Cozzarelli, N.R. (2005). A genetic selection for supercoiling mutants of Escherichia coli reveals proteins implicated in chromosome structure. Mol. Microbiol. *57*, 1636–1652.

Hebenstreit, D. (2013). Are gene loops the cause of transcriptional noise? Trends Genet. *29*, 333–338.

Herbert, K.M., La Porta, A., Wong, B.J., Mooney, R.A., Neuman, K.C., Landick, R., and Block, S.M. (2006). Sequence-resolved detection of pausing by single RNA polymerase molecules. Cell *125*, 1083–1094.

Herbert, K.M., Greenleaf, W.J., and Block, S.M. (2008). Single-molecule studies of RNA polymerase: motoring along. Annu. Rev. Biochem. *77*, 149–176.

Higgins, N.P., and Cozzarelli, N.R. (1982). The binding of gyrase to DNA: analysis by retention by nitrocellulose filters. Nucleic Acids Res. *10*, 6833–6847.

Higgins, N.P., Peebles, C.L., Sugino, A., and Cozzarelli, N.R. (1978). Purification of subunits of Escherichia coli DNA gyrase and reconstitution of enzymatic activity. Proc. Natl. Acad. Sci. USA *75*, 1773–1777.

Hocine, S., Raymond, P., Zenklusen, D., Chao, J.A., and Singer, R.H. (2013). Single-molecule analysis of gene expression using two-color RNA labeling in live yeast. Nat. Methods *10*, 119–121.

Hodges, C., Bintu, L., Lubkowska, L., Kashlev, M., and Bustamante, C. (2009). Nucleosomal fluctuations govern the transcription dynamics of RNA polymerase II. Science *325*, 626–628.

Kannemeier, C., Shibamiya, A., Nakazawa, F., Trusheim, H., Ruppert, C., Markart, P., Song, Y., Tzima, E., Kennerknecht, E., Niepmann, M., et al. (2007). Extracellular RNA constitutes a natural procoagulant cofactor in blood coagulation. Proc. Natl. Acad. Sci. USA *104*, 6388–6393.

Kapanidis, A.N., Margeat, E., Ho, S.O., Kortkhonjia, E., Weiss, S., and Ebright, R.H. (2006). Initial transcription by RNA polymerase proceeds through a DNA-scrunching mechanism. Science *314*, 1144–1147.

Kussell, E., and Leibler, S. (2005). Phenotypic diversity, population growth, and information in fluctuating environments. Science *309*, 2075–2078.

Landick, R. (2006). The regulatory roles and mechanism of transcriptional pausing. Biochem. Soc. Trans. *34*, 1062–1066.

Larson, D.R., Zenklusen, D., Wu, B., Chao, J.A., and Singer, R.H. (2011). Real-time observation of transcription initiation and elongation on an endogenous yeast gene. Science *332*, 475–478.

Leng, F., Chen, B., and Dunlap, D.D. (2011). Dividing a supercoiled DNA molecule into two independent topological domains. Proc. Natl. Acad. Sci. USA *108*, 19973–19978.

Li, G.W., and Xie, X.S. (2011). Central dogma at the single-molecule level in living cells. Nature *475*, 308–315.

Lim, H.M., Lewis, D.E., Lee, H.J., Liu, M., and Adhya, S. (2003). Effect of varying the supercoiling of DNA on transcription and its regulation. Biochemistry *42*, 10718–10725.

Lionberger, T.A., and Meyhöfer, E. (2010). Bending the rules of transcriptional repression: tightly looped DNA directly represses T7 RNA polymerase. Biophys. J. *99*, 1139–1148.

Lionnet, T., Czaplinski, K., Darzacq, X., Shav-Tal, Y., Wells, A.L., Chao, J.A., Park, H.Y., de Turris, V., Lopez-Jones, M., and Singer, R.H. (2011). A transgenic mouse for in vivo detection of endogenous labeled mRNA. Nat. Methods *8*, 165–170.

Liu, L.F., and Wang, J.C. (1987). Supercoiling of the DNA template during transcription. Proc. Natl. Acad. Sci. USA *84*, 7024–7027.

Lynch, A.S., and Wang, J.C. (1993). Anchoring of DNA to the bacterial cytoplasmic membrane through cotranscriptional synthesis of polypeptides encoding membrane proteins or proteins for export: a mechanism of plasmid hypernegative supercoiling in mutants deficient in DNA topoisomerase I. J. Bacteriol. *175*, 1645–1655.

Ma, J., Bai, L., and Wang, M.D. (2013). Transcription under torsion. Science *340*, 1580–1583.

Maamar, H., Raj, A., and Dubnau, D. (2007). Noise in gene expression determines cell fate in Bacillus subtilis. Science *317*, 526–529.

Maxwell, A., and Gellert, M. (1984). The DNA dependence of the ATPase activity of DNA gyrase. J. Biol. Chem. *259*, 14472–14480.

Mitarai, N., Dodd, I.B., Crooks, M.T., and Sneppen, K. (2008). The generation of promoter-mediated transcriptional noise in bacteria. PLoS Comput. Biol. *4*, e1000109.

Morrison, A., and Cozzarelli, N.R. (1981). Contacts between DNA gyrase and its binding site on DNA: features of symmetry and asymmetry revealed by protection from nucleases. Proc. Natl. Acad. Sci. USA *78*, 1416–1420.

Munsky, B., Neuert, G., and van Oudenaarden, A. (2012). Using gene expression noise to understand gene regulation. Science *336*, 183–187.

Muramoto, T., Cannon, D., Gierlinski, M., Corrigan, A., Barton, G.J., and Chubb, J.R. (2012). Live imaging of nascent RNA dynamics reveals distinct types of transcriptional pulse regulation. Proc. Natl. Acad. Sci. USA *109*, 7350–7355.

Ozbudak, E.M., Thattai, M., Kurtser, I., Grossman, A.D., and van Oudenaarden, A. (2002). Regulation of noise in the expression of a single gene. Nat. Genet. *31*, 69–73.

Pedraza, J.M., and Paulsson, J. (2008). Effects of molecular memory and bursting on fluctuations in gene expression. Science *319*, 339–343.

Peter, B.J., Arsuaga, J., Breier, A.M., Khodursky, A.B., Brown, P.O., and Cozzarelli, N.R. (2004). Genomic transcriptional response to loss of chromosomal supercoiling in Escherichia coli. Genome Biol. *5*, R87.

Postow, L., Hardy, C.D., Arsuaga, J., and Cozzarelli, N.R. (2004). Topological domain structure of the Escherichia coli chromosome. Genes Dev. *18*, 1766–1779.

Raj, A., Peskin, C.S., Tranchina, D., Vargas, D.Y., and Tyagi, S. (2006). Stochastic mRNA synthesis in mammalian cells. PLoS Biol. *4*, e309.

Raj, A., Rifkin, S.A., Andersen, E., and van Oudenaarden, A. (2010). Variability in gene expression underlies incomplete penetrance. Nature *463*, 913–918.

Raser, J.M., and O'Shea, E.K. (2004). Control of stochasticity in eukaryotic gene expression. Science *304*, 1811–1814.

Rau, D.C., Gellert, M., Thoma, F., and Maxwell, A. (1987). Structure of the DNA gyrase-DNA complex as revealed by transient electric dichroism. J. Mol. Biol. *193*, 555–569.

Reece, R.J., and Maxwell, A. (1991). DNA gyrase: structure and function. Crit. Rev. Biochem. Mol. Biol. *26*, 335–375.

Revyakin, A., Ebright, R.H., and Strick, T.R. (2004). Promoter unwinding and promoter clearance by RNA polymerase: detection by single-molecule DNA nanomanipulation. Proc. Natl. Acad. Sci. USA *101*, 4776–4780.

Revyakin, A., Zhang, Z., Coleman, R.A., Li, Y., Inouye, C., Lucas, J.K., Park, S.R., Chu, S., and Tjian, R. (2012). Transcription initiation by human RNA polymerase II visualized at single-molecule resolution. Genes Dev. *26*, 1691–1702.

Rovinskiy, N., Agbleke, A.A., Chesnokova, O., Pang, Z., and Higgins, N.P. (2012). Rates of gyrase supercoiling and transcription elongation control supercoil density in a bacterial chromosome. PLoS Genet. *8*, e1002845.

Samul, R., and Leng, F. (2007). Transcription-coupled hypernegative supercoiling of plasmid DNA by T7 RNA polymerase in Escherichia coli topoisomerase I-deficient strains. J. Mol. Biol. *374*, 925–935.

Shundrovsky, A., Santangelo, T.J., Roberts, J.W., and Wang, M.D. (2004). A single-molecule technique to study sequence-dependent transcription pausing. Biophys. J. *87*, 3945–3953.

Singh, A., Razooky, B., Cox, C.D., Simpson, M.L., and Weinberger, L.S. (2010). Transcriptional bursting from the HIV-1 promoter is a significant source of stochastic noise in HIV-1 gene expression. Biophys. J. *98*, L32–L34.

Skinner, G.M., Baumann, C.G., Quinn, D.M., Molloy, J.E., and Hoggett, J.G. (2004). Promoter binding, initiation, and elongation by bacteriophage T7 RNA polymerase. A single-molecule view of the transcription cycle. J. Biol. Chem. *279*, 3239–3244.

Snyder, M., and Drlica, K. (1979). DNA gyrase on the bacterial chromosome: DNA cleavage induced by oxolinic acid. J. Mol. Biol. *131*, 287–302.

So, L.H., Ghosh, A., Zong, C., Sepúlveda, L.A., Segev, R., and Golding, I. (2011). General properties of transcriptional time series in Escherichia coli. Nat. Genet. *43*, 554–560.

Suter, D.M., Molina, N., Gatfield, D., Schneider, K., Schibler, U., and Naef, F. (2011). Mammalian genes are transcribed with widely different bursting kinetics. Science *332*, 472–474.

Tang, G.Q., Roy, R., Bandwar, R.P., Ha, T., and Patel, S.S. (2009). Real-time observation of the transition from transcription initiation to elongation of the RNA polymerase. Proc. Natl. Acad. Sci. USA *106*, 22175–22180.

Taniguchi, Y., Choi, P.J., Li, G.W., Chen, H., Babu, M., Hearn, J., Emili, A., and Xie, X.S. (2010). Quantifying E. coli proteome and transcriptome with single-molecule sensitivity in single cells. Science *329*, 533–538.

ten Heggeler-Bordier, B., Wahli, W., Adrian, M., Stasiak, A., and Dubochet, J. (1992). The apical localization of transcribing RNA polymerases on supercoiled DNA prevents their rotation around the template. EMBO J. *11*, 667–672.

Thattai, M., and van Oudenaarden, A. (2004). Stochastic gene expression in fluctuating environments. Genetics *167*, 523–530.

Tsao, Y.P., Wu, H.Y., and Liu, L.F. (1989). Transcription-driven supercoiling of DNA: direct biochemical evidence from in vitro studies. Cell *56*, 111–118.

Wang, W., Li, G.W., Chen, C., Xie, X.S., and Zhuang, X. (2011). Chromosome organization by a nucleoid-associated protein in live bacteria. Science *333*, 1445–1449.

Weixlbaumer, A., Leon, K., Landick, R., and Darst, S.A. (2013). Structural basis of transcriptional pausing in bacteria. Cell *152*, 431–441.

Willmott, C.J., Critchlow, S.E., Eperon, I.C., and Maxwell, A. (1994). The complex of DNA gyrase and quinolone drugs with DNA forms a barrier to transcription by RNA polymerase. J. Mol. Biol. *242*, 351–363.

Wolf, D.M., Vazirani, V.V., and Arkin, A.P. (2005). Diversity in times of adversity: probabilistic strategies in microbial survival games. J. Theor. Biol. *234*, 227–253.

Wu, H.Y., Shyy, S.H., Wang, J.C., and Liu, L.F. (1988). Transcription generates positively and negatively supercoiled domains in the template. Cell *53*, 433–440.

Zhang, Z., Revyakin, A., Grimm, J.B., Lavis, L.D., and Tjian, R. (2014). Single-molecule tracking of the transcription cycle by sub-second RNA detection. eLife *3*, e01775.

Zong, C., So, L.H., Sepúlveda, L.A., Skinner, S.O., and Golding, I. (2010). Lysogen stability is determined by the frequency of activity bursts from the fate-determining gene. Mol. Syst. Biol. *6*, 440.

EXTENDED EXPERIMENTAL PROCEDURES

Construction of In Vitro Transcription Templates

T7 promoter sequence was placed at the 5′ end of a 12 kb DNA sequence (*E. coli* operon *nuoB-N*) by PCR. *E. coli* RNApol T7A1 promoter was placed at the 5′ end of a 12 kb DNA sequence (*E. coli* operon *ftsL-murC*) by PCR. The linear T7 or *E. coli* transcription template containing a single biotinylated nucleotide was made by PCR with 5′-end biotinylated primer (Integrated DNA Technologies). We made a DNA fragment with multiple biotinylated nucleotides by performing PCR using a 200 bp template with arbitrary sequence, corresponding primers at both ends and dNTP mix with equal concentration of regular dTTP and biotin-16-dUTP (Biotium, Hayward, CA) (Revyakin et al., 2005). The linear transcription template with multiple biotinylated nucleotides on both strands at the 3′ end was made through ligation between a 12 kb transcribing sequence and the 200 bp biotinylated fragment, followed by purification using AmPure beads (Agencourt, Beckman Coulter, Pasadena, CA).

In order to make the circular transcription templates, a linear T7 or *E. coli* transcription unit was first made by PCR, which consists of a 5′-end T7 or T7A1 promoter, a 12 kb-long transcribing sequence and a 3′-end T7 or *E. coli* rrnD terminator adapted from pET30a expression plasmid (Addgene) or *E. coli* chromosome, respectively. The termination efficiency of T7 and rrnD terminator is both > 90% (Cambray et al., 2013; Telesnitsky and Chamberlin, 1989). The final circular template was made by two sequential ligation steps. The first ligation was between the linear transcription unit and the 200 bp biotinylated fragment, and the second was an intramolecular circularization. The final self-looping product was purified using λ exonuclease (New England Biolabs) and AmPure beads.

DNA Supercoiling and Relaxation Assays

The DNA supercoiling reaction mixture (21 μL) contained the following components: 1 unit of *E. coli* gyrase (New England Biolabs), 0.7 μg relaxed pUC19 (New England Biolabs), 1.75 mM ATP, 0.3 mM C/G/UTP and transcription buffer (40 mM Tris-HCl, pH 8.0, 10 mM $MgCl_2$, 5 mM DTT, 50 mM KCl, 6.5% glycerol and 100 μg/mL BSA) with or without 250 nM SYTO RNASelect (Life Technologies). The mixture was incubated at 37°C for 10, 20, 30, 40 or 60 min. The reaction was stopped with 4.2 μl of quench buffer (500 mM EDTA). After the reaction, pUC19 was purified (D4004, Zymo Research, Irvine, CA), and its supercoiling level was probed by DNA agarose gel electrophoresis and SYBR Safe (Life Technologies) staining (Figure S1A). The fraction of negatively supercoiled pUC19 after each gyrase reaction was measured from the intensity ratio of corresponding bands in the DNA gel image. Figure S1C shows the fraction as a function of gyrase reaction time, indicating that 250 nM SYTO RNASelect does not affect the activity of gyrase.

The DNA relaxation assay mixture (12.5 μL) contained the following components: 0.25 unit of *E. coli* Topo I (New England Biolabs, Ipswich, MA), 0.5 μg negatively supercoiled pUC19, 1.75 mM ATP, 0.3 mM C/G/UTP and transcription buffer with or without 250 nM SYTO RNASelect. We note NTPs were not necessary for the Topo I activity. They were present to mimic the condition of the single-molecule transcription assay. The mixture was incubated at 37°C for 3, 6, 9, 15 or 30 min. The reaction was stopped with 1.5 μl of quench buffer (500 mM EDTA). The supercoiling level of the purified pUC19 was examined by DNA agarose gel as in the DNA supercoiling assay (Figure S1B). The fraction of relaxed pUC19 after each Topo I reaction was measured from the intensity ratio of corresponding bands in the DNA gel image. Figure S1D shows the fraction as a function of Topo I reaction time, indicating that 250 nM SYTO RNASelect does not affect the activity of Topo I.

Ensemble In Vitro Transcription Assay

To probe potential SYTO RNASelect dye effect on in vitro transcription, an ensemble transcription assay was assembled by mixing T7 RNA polymerase (New England Biolabs) or *E. coli* RNA polymerase (Epicentre Technologies Corp., Chicago, IL), NTPs, and DNA templates containing corresponding promoter and a 5.3 kb transcribing sequence (*E. coli lac* operon), with or without 250 nM dye addition. RNase Inhibitor, Murine (New England Biolabs) was added to prevent RNA degradation during reaction. The reaction mixture was incubated at 37°C for 2 hr. Afterward, the template DNA was removed by TURBO DNase treatment (Life Technologies). The length and amount of the RNA product were probed by formaldehyde-based RNA agarose gel electrophoresis and EtBr straining. Figure S1H and S1G shows that neither T7 transcription nor *E. coli* transcription was affected by the presence of 250 nM SYTO RNASelect.

To further test potential SYTO RNASelect dye effect on the in vitro transcription rate, a real-time transcription assay was carried out with RNA yield measured at 6 time points within the first 30 min of transcription reaction. The ensemble transcription assay recipe was the same as described above, except the final RNA product was purified by RNA purification column (Zymo Research) and quantified by Qubit RNA HS assay (Life Technologies). As shown in Figure S1E and S1F, 250 nM SYTO RNASelect does not affect transcription rates of T7 or *E. coli* RNApol.

To test potential surface effect on our in vitro transcription system, we attached 12 kb-long linear DNA templates used in the in vitro single-molecule transcription assay to Dynabeads MyOne Streptavidin T1 (Life Technologies) following the standard protocol in the instruction. After washing the DNA attached beads, an ensemble in vitro transcription assay was assembled by mixing the beads with T7 RNA polymerase and NTPs. RNase Inhibitor was added to prevent RNA degradation. After 2 hr incubation at 37°C, the beads were removed from the reaction mixture using a magnetic bar, and the product in the solution was purified by a RNA purification column (Zymo Research) and further analyzed by formaldehyde-based RNA agarose gel electrophoresis and EtBr staining. Figure S1I shows

that T7 transcription on the linear templates tethered to the bead surface with either single or multiple biotin-streptavidin linkages produce full-length transcripts, suggesting our in vitro transcription system is robust and not significantly affected by template attachment to surface.

SYTO RNASelect Fluorescence Spectra

The fluorescence emission spectra of SYTO RNASelect were measured under 488 nm excitation (Varian Cary Eclipse Fluorimeter, Agilent Technologies, Santa Clara, CA) in the transcription buffer at a dye concentration of 10 μM under three conditions (Figure 2B): in the absence of nucleic acids, in the presence of 60 ng/μL lambda DNA, or in the presence of 60 ng/μL 4 kb-long RNA prepared from T7 transcription from lambda DNA template.

In Vitro Single-Molecule Transcription Assay

The in vitro single-molecule transcription assay was performed inside a flow cell. For room-temperature experiments, coverslip surface treatment and flow cell construction were performed as previously described (Kim et al., 2007; Kim et al., 2013; Schroeder et al., 2008). The difference in coverslip surface treatment from the pervious procedure is that the PEG polymer solution used for surface functionalization was composed of 100 mg/mL mPEG-Succinimidyl Valerate (MW 5000, Laysan Bio, Arab, AL), 10 mg/mL SVA-mPEG-SVA (MW 3400, Laysan Bio) and 4 mg/mL biotin-mPEG-SVA (MW 5000, Laysan Bio). Compared with T7 RNApol, the activity of *E. coli* RNApol was found to be more sensitive to the storage condition of functionalized coverslips. Successful performance of in vitro single-molecule transcription assay with *E. coli* RNApol required the use of functionalized coverslips that were either freshly prepared or preserved at −80°C in vacuum that was generated by a foodsaver vacuum sealer.

For measurements at 37°C, a flow cell was constructed using a round coverslip (40 mm diameter) with the same surface treatment and a microaqueduct slide originally used in a live-cell micro-observation chamber system (FCS2, Bioptechs, Butler, PA). The flow cell temperature was controlled with the electronic controller in the FCS2 system.

An inverted microscope (Olympus IX70, Olympus America, Melville, NY) was used for objective-type total internal reflection (TIR) illumination. A focused beam of 488 nm Argon laser (Innova300C MotoFreD, Coherent) was directed at the edge of the back focal plane of a 60x objective lens (numerical aperture 1.45; PlanApo, Olympus) after passing through an excitation filter (L-488-10, Thin Film Imaging Technologies, Greenfield, MA). Excitation was controlled by a shutter (VS25S2ZM1R1-24, Vincent Associates, Rochester, NY). Fluorescence was collected through the same objective lens. After passing through an emission filter (HQ535/30M, Chroma, Bellows Falls, VT), the fluorescence was imaged on a back-illuminated electron multiplying charge coupled device camera (iXonEM+897, Andor Technology, South Windsor, CT). Typically, a field of view contained 300-600 immobilized DNA molecules in ~110 × 110 μm^2.

In order to measure T7 transcription elongation rates at room temperature, 5.3 nM T7 RNApol (New England Biolabs), 1.75 mM ATP, 0.3 mM C/G/UTP, 250 nM SYTO RNASelect and an O_2-scavenging system (0.1 mg/mL glucose oxidase, 0.023 mg/mL catalase and 8 mg/mL dextrose) were added to 200 μl transcription buffer. To measure *E. coli* transcription elongation rates at 37°C, the reaction mixture was the same as T7 transcription except that it contained 220 nM *E. coli* RNApol (Epicentre) instead of T7 RNApol. Immediately after the mixture was infused into the flow cell containing immobilized DNA templates, a fluorescent movie was recorded under 488 nm laser excitation at 0.22 W/cm^2. Images were taken every 20 s for 60-80 min with an image acquisition time of 5 s.

In order to measure T7 transcription initiation rates at 37°C, the reaction mixture was the same as that for T7 transcription elongation rate measurements except that concentrations of T7 RNApol and C/G/UTP were increased to 36.1 nM and 0.8 mM, respectively. To measure *E. coli* transcription initiation rates at 37°C, 176 nM *E. coli* RNApol, 3 mM A/C/G/UTP, 250 nM SYTO RNASelect and O_2-scavenging system composed of 2.5 mM protocatechuic acid (PCA, from Sigma-Aldrich, St. Louis, MO) and 50 nM protocatechuate-3,4-dioxygenase (PCD, from Sigma-Aldrich) were added to 40 μl transcription buffer. *E. coli* transcription initiation was found to be faster in the presence of the PCA/PCD O_2-scavenging system than in the presence of the glucose oxidase/catalase system. Fluorescent movies were recorded under 488 nm laser excitation at 0.15 W/cm^2. Images were taken every 75 s with an image acquisition time of 5 s.

DNA Staining Assay

In order to locate the linear and circular templates in the field of view, 100 nM SYTOX Orange (Life Technologies) in 50 mM Tris-HCl buffer (pH 8.0) was used to stain the immobilized DNAs after transcription movies were recorded. Fluorescent movies were recorded under excitation of a 532 nm diode laser (UGA-250; LambdaPro, Beijing) with a power density at the focal plane above 4 W/cm^2 and an image acquisition time of 0.3 s.

The imaging buffer was kept flowing at 8 mL/hr by a syringe pump (PhD 2000, Harvard Apparatus, Holliston, MA) during the movie recording. Circular and linear DNAs with the same length were stretched to different extents under flow. With the sufficiently high laser power, the stained DNAs underwent stepwise photocleavage. A circular DNA was cut to become two linear ones that were subsequently shortened, whereas a linear DNA was shortened from the beginning (Figure S3). We identified the shape of each DNA molecule in the field of view by eyeballing the photocleavage events. Some DNA molecules appeared not freely stretched under flow after 2.5 hr of *E. coli* transcription in the measurements of initiation rate. 1 ml of 2.5 M KCl solution was used to rinse the flow cell after the *E. coli* transcription assays before DNA staining.

Single-Molecule Data analysis to Measure Transcription Elongation and Initiation Rates

By overlaying an RNA movie with its corresponding DNA movie, the positions of effective DNA templates were identified in the RNA movie. For each DNA template, the fluorescence intensity in an RNA image was integrated over a 5-pixel-by-5-pixel area surrounding the DNA position. By plotting the intensity against the time when the RNA image was acquired, we generated the intensity trajectory for the template (see Figure 2D and S4A for examples).

The intensity versus time trajectory of a template is composed of multiple peaks, each corresponding to one transcript. Under the conditions of transcription elongation rate measurements, peaks are far separated from each other in time. The elongation rate equals to the known length of a transcript divided by the elongation time, that is, the time it takes the intensity of a transcript to rise from bottom to peak. The elongation rate under each condition was averaged from measurements of over 300 individual transcripts, with an error bar obtained by the bootstrapping method (Efron and Tibshirani, 1993).

Under steady-state conditions, transcription initiation rate at a specific time point is proportional to the sum of RNA intensity produced from a population of templates. Plotting the total RNA intensity as a function of time under a given condition includes three steps. First, we picked all the effective templates in a field of view and extracted the intensity trajectory for each of them. In order to get enough number of effective templates (>100), we performed each time-lapse measurement for multiple times. Second, we subtracted the background, i.e., the average intensity outside "peaks," from the trajectory. The background intensity is contributed from free dye in the solution and the immobilized DNA that is weakly fluorescent (Figure 2B). After the subtraction, the remaining intensity is only from nascent RNA. Finally, we plotted the sum of intensity from all the background-free trajectories as a function of time. For T7 and *E. coli* transcription, the bin size of time was 225 s and 375 s, respectively.

There was always a mixture of linear and circular templates immobilized on the flow cell surface in our measurement of transcription initiation rates. While circular templates were used to study the effect of supercoiling accumulation on transcription initiation, linear templates served as probes of transcription initiation rate when supercoiling accumulation did not play a role. The time-dependent total intensity of linear templates reflected intrinsic variation of initiation rate during the in vitro measurement due to temperature, effective RNApol concentration, NTPs and pyrophosphate concentrations, degradation of the functionalized surface, etc. While the intrinsic variation of initiation rate over 9000 s was small for T7 transcription, the variation was significant for *E. coli* transcription. Therefore we normalized the intensity from circular templates to that from linear templates in order to study the effect of positive supercoiling accumulation on *E. coli* transcription initiation rate.

In order to depict the time dependence of *E. coli* transcription initiation rate (Figure 4G and S5), we first got the average intensity versus time from one circular and linear template by dividing the total intensity at each time point by the number of templates, respectively. Then we normalized the average intensity from one circular template at each time point to that from one linear template. The number of circular and linear templates measured for each condition is noted in the corresponding figure caption.

To depict time dependence of T7 transcription initiation rate (Figure 4B, D&F), we normalized the total RNA intensity from 160 circular templates to constant fluorescence intensity 1.2×10^6. Yet in order to accurately measure the recovery rate constant of T7 transcription initiation due to supercoiling release, we normalized the average intensity from circular templates to that from linear templates (Figure 5B).

Control for Photobleaching of SYTO RNASelect Stained with RNA

Coverslip surface treatment and flow cell construction were performed as previously described (Kim et al., 2013). 4 kb-long RNA was prepared by ensemble in vitro T7 transcription. The 3′ end of the RNA was hybridized to a 40-mer complementary DNA that contained a single biotinylated nucleotide. The biotinylated RNA molecules were immobilized on the flow cell surface and stained with 250 nM SYTO RNASelect in the transcription buffer mixed with a fresh glucose oxidase/catalase O_2-scavenging system (Figure S2A). The fluorescent movie was recorded for 300 s under continuous 488 nm laser excitation at 0.22 W/cm^2. The acquisition time of each image was 5 s. The total illumination time was the same as that of a 1200 s movie for transcription elongation rate measurement, where images were taken every 20 s. We note that 1200 s is significantly longer than the average time for generating a full transcript of 12 kb (Figure 3B). Single RNA molecules appear as individual fluorescent spots in the field of view. The total fluorescence intensity versus time trajectory of 67 individual RNA molecules was extracted from the 300 s movie (Figure S2B), which directly measures photobleaching of stained RNA, if any, during the time of transcription elongation. The O_2-scavenging effect of the PCA/PCD system used in the measurement of *E. coli* transcription initiation rates is comparable to that of the glucose oxidase/catalase system (Aitken et al., 2008).

Control for DNA Photocleavage in the Presence of SYTO RNASelect

Negatively supercoiled pUC19 DNA was prepared by incubating relaxed pUC19 (New England Biolabs) with *E. coli* gyrase. The sample for the photocleavage assay was a mixture of 5 μg/ml negatively supercoiled pUC19, 250 nM SYTO RNASelect and a fresh glucose oxidase/catalase O_2-scavenging system in the transcription buffer, mimicking the condition for the in vitro single-molecule transcription assay. The solution was filled in a quartz spectrophotometer cuvette (16.40F-Q-10, Starna Cells, Atascadero, CA) with three clear windows, two of which are square ones on the opposite sides of the cuvette. A collimated laser beam at 488 nm was aligned with the square windows, which continuously excited the solution at 0.22 W/cm^2 or 7.3 W/cm^2 for 30 min. The power density of 0.22 W/cm^2 was used for in the in vitro single-molecule assay. The total illumination time was longer than that for in vitro transcription elongation and initiation rate measurements.

After illumination, pUC19 was purified with a DNA purification column (QIAGEN). The supercoiling level of the DNA was probed by agarose gel electrophoresis with SYBR Safe strain (Life Technologies), which displays the mobility difference among supercoiled, nicked and linear DNA (Tycon et al., 2012), the latter two are products of DNA photocleavage. Figure S2C shows that minimal DNA photocleavage occurred under our experimental conditions.

Number of Transcripts Leading to Inhibition of Transcription Initiation through Positive Supercoiling Accumulation In Vitro

In order to measure the fluorescence intensity generated by one transcript, we performed in vitro single-molecule transcription assay under the same conditions as for measurements of T7 or *E. coli* transcription initiation rates in the absence of topoisomerases, except that the T7 and *E. coli* RNApol concentration was reduced to 2.2 nM and 22 nM, respectively. With the low concentration of RNApol, transcription events on a circular DNA template were well separated temporally. Figure S4A shows examples of fluorescence intensity versus time trajectories of T7 transcription. One round of T7 transcription appears as a "spike" in the trajectory, and it takes 1.9 points on average for the fluorescence intensity to increase from bottom to top, according to analysis of 226 spikes from 56 trajectories. The sum of intensity from all the points in a spike is the fluorescence intensity generated by one full transcript.

Averaging from the 226 individual transcripts, the fluorescence intensity of one full transcript was determined to be $(13.5 \pm 1.49) \times 10^3$. The error bar was obtained by the bootstrapping method (Efron and Tibshirani, 1993). Since the total intensity generated from 160 circular templates between the moments of Topo I addition and transcription initiation inhibition (~20% of initial value) was 2.04×10^7 (Figure S4B), the average number of transcripts leading to the inhibition of transcription initiation on a single template was 9.44 ± 1.05.

Averaging from 142 individual transcripts produced by *E. coli* transcription, the fluorescence intensity of one full transcript was determined to be $(16.1 \pm 3.24) \times 10^4$. The transcript intensity was higher than that generated by T7 transcription, because of a lower *E. coli* transcription elongation rate and a lower termination rate under our in vitro condition, leading to a longer imaging time of a nascent transcript. The total intensity generated from 106 circular templates between the moments of Topo I addition and transcription initiation inhibition (~25% of initial value) was 9.13×10^7. Thus the average number of transcripts leading to the inhibition of initiation on a single template was 5.33 ± 1.07.

Number of T7 Transcripts Simultaneously Elongating on a DNA Template In Vitro

We can estimate the number of T7 transcripts simultaneously elongating on a DNA template by comparing the average interval between transcription initiation events on a single template with the average elongation time of a transcript. If the former is significantly larger than the latter, then most of the time there is zero or one transcript elongating on a template.

As calculated previously, 9.44 transcripts generated from a single DNA template lead to enough positive supercoiling accumulation that inhibits T7 transcription initiation. According to Figure S4B, it takes 5850 s to generate these transcripts. Therefore the average interval between transcription initiation events on a single template is 5850/9.44 = 620 s.

In the absence of topoisomerases (steady state 1), the total fluorescence intensity generated from 160 circular templates during 5850 s was 3.23×10^7 (Figure S4C), the number of T7 transcripts per template is 15.0, and the average transcription initiation interval on a single template is 390 s. In the presence of both Topo I and gyrase (steady state 2), the total intensity from 160 circular templates during 5850 s was 3.14×10^7 (Figure S4D), the number of T7 transcripts per template is 14.6, and the average transcription initiation interval on a single template is 401 s.

We note that the initiation rates of steady state 1 and 2 were the same because with such a combination of T7 RNApol, Topo I and gyrase concentrations in steady state 2, positive supercoiling was generated as fast as it was released. The circular templates remained to be relaxed during the measurement. We have used 33 nM or 66 nM gyrase in the initiation rate measurement with both Topo I and gyrase, besides 100 nM gyrase as shown in Figure 4D and S4D. With a lower gyrase concentration, positive supercoiling was generated faster than it was released and circular templates remained to be slightly positively supercoiled. The steady state initiation rate with 33 nM or 66 nM gyrase (data not shown) was higher than the final state in Figure S4B and lower than that of steady state 1 (Figure S4C) or steady state 2 (Figure S4D).

The fluorescent movies for transcription initiation rate measurements were recorded with a low temporal resolution (one frame every 75 s), which does not allow accurate measurement of transcription elongation rates. However, the number of points it takes for fluorescence intensity to increase from bottom to top within a "spike" on the single-molecule trace provides an estimation of the total elongation time of a transcript. Since the average number of points is 1.9, the average elongation time of a T7 transcript is < 150 s, much smaller than the T7 transcription initiation interval on a single template under all three conditions as calculated above. In conclusion, most of the time there is zero or only one T7 transcript elongating on a DNA template under our in vitro experimental conditions.

K_d of Gyrase-DNA Complex Determined from Gyrase Concentration Dependence of Transcription Elongation Rates

In the presence of gyrase, the observed T7 transcription elongation rate R_{obs} on multiple-biotin templates (Figure 3C) is an average from a subpopulation of DNA templates with effective gyrase binding and a subpopulation of free DNA templates, which differ in elongation rates. We assign the elongation rate on a free multiple-biotin DNA template to be R_D and the elongation rate on a

gyrase-bound multiple-biotin DNA template to be R_{DG}. If the percentage of gyrase-bound DNA is x, then the average elongation rate R_{obs} is

$$R_{obs} = (1 - x)R_D + xR_{DG}.$$

Accordingly, when R_{obs} reaches half of the plateau value in the titration experiment, that is

$$R_{obs} = 0.5(R_D + R_{DG}),$$

50% of all the DNAs are gyrase-bound, the corresponding gyrase concentration equals to K_d. From Figure 3C, K_d of gyrase-DNA complex is approximately 100 nM.

In a live *E. coli* cell, there are comparable number of gyrase molecules and chromosomal DNA loops (400∼500) in a cell volume V, where V is ∼0.6 μm^3 (Kubitschek, 1990). For simplicity, we take 450 as the intracellular number of both molecules. Many gyrase molecules are trapped on chromosomal DNA loops. Assuming a DNA loop has one gyrase molecule binding at a time, there are the same number (X) of unbound gyrase molecules and unbound DNA loops. Based on the definition of dissociation constant of gyrase-DNA complex, we have

$$K_d = \frac{(X/N_A/V)^2}{(450 - X)/N_A/V}, \quad \text{(Eq. S1)}$$

where N_A is the Avogadro constant. By solving Eq. S1, we get X equals to 111, which corresponds to an intracellular concentration of 0.3 μM. This is 25% of the total gyrase concentration. For a specific DNA loop, the fraction of time when it is unbound to gyrase is 25%.

Bacterial Genetic Constructs

The *lac* operon of *E. coli* strain BW25993 was fused endogenously to *yfp* (*venus)* gene (Nagai et al., 2002) at the 3′ end of *lacY* gene via λ-red recombination (Datsenko and Wanner, 2000). The kanamycin resistant gene used for screening was subsequently removed via FRT recombination (Datsenko and Wanner, 2000). A strong gyrase site (SGS) nuB1 sequence (Pato et al., 1990) was inserted upstream of the *lac* operon also via λ-red recombination, where the *lacY* gene was already tagged with *venus* gene. The 18 library strains with *venus* fused to the 3′ end of each target gene were obtained from our YFP library from previous work (Taniguchi et al., 2010).

The plasmid-borne *lac* operon expression system was made by inserting the whole *lac* operon sequence (including the *lacI* gene and *venus* fusion with *lacY*) into a single-copy plasmid backbone pVS133 based on the *parABC* partitioning system. The plasmid was then electroporated into *Δlac* BW25993 bacterial cells and maintained by carbernicillin resistance. We note that even with the partition system, there might be cells with 2 plasmids occasionally. This gene dosage variation may slightly contribute to the nonPoissonian mRNA distribution.

The gyrase overexpression plasmid was made based on a pBAD expression system with kanamycin resistance. *E. coli* genes *gyrA* and *gyrB* were placed in a polycistronic manner, using their original ribosome binding sites to maintain physiological stoichiometry of the two subunits. A final 0.2% L-arabinose (Sigma-Aldrich) was used to induce gyrase overexpression from the plasmid.

Rifampicin Assay

At time zero, 500 ng/μL rifampicin was added to stop transcription initiation but not on-going elongation. 10 ng/μL norfloxacin was added simultaneously to inhibit gyrase activity in the cell. 8 cell samples were taken out and immediately fixed for later mRNA quantification analysis at multiple time points with 2 min interval, at 0, 2, 4, 6, 8 10, 12, 14 min following the drug treatment, respectively. The mRNA abundance of the 7 probes along *lac* operon from 5′ end to 3′ end was measured for all 8 samples, as shown in log scale in Figure 6C. A final result of the transcription elongation rate measurement was shown in Figure 6D. The protocol is adapted from H. Chen, K. Shiroguchi, H.G., and X.S.X. (unpublished data).

Bacterial mRNA Extraction and Quantitative RT-PCR

Upon harvest, 1/10 volume of ice-cold 90:10 ethanol:phenol mixture was added to the cells followed by centrifuge and PBS wash. The cells were then lysed by lysozyme treatment and supplemented with spike-in RNA for absolute quantification. RNA was purified from the cell lysis by phenol:chloroform extraction, isopropanol precipitation and 70% ethanol wash for several times. Following DNA removal by DNase I treatment, RNA product was purified with a purification column (R1015, Zymo Research), quantified (Nanodrop 2000, Thermo Fisher Scientific, Waltham, MA) and converted to cDNA by M-MuLV reverse transcription (New England Biolabs). Quantitative RT-PCR was performed to determine the mRNA amount using SYBR qPCR Master Mix and ROX dye (Finnzymes, Thermo Fisher Scientific).

Killing Curve Measurement upon Drug Treatment

LB plating and colony counting following serial dilution in LB medium was used to measure the *E. coli* cell killing curve upon 10 ng/μL norfloxacin treatment (Figure S6A), which was the same condition as the rifampicin assay for live-cell transcription elongation rate measurement. Figure S6A shows that the cell number was almost constant within the first 20 min after drug treatment, and decreased

afterward. Since our rifampicin assay was performed within the first 14 min after norfloxacin treatment, cell death was not a major issue and would not affect final results.

Growth Rate Measurement upon Drug Treatment

OD_{600nm} was measured to monitor the growth rate upon novobiocin treatment at various concentrations, and the doubling time was calculated from the initial OD value, the final OD value and the incubation time in between. Cells were grown at 37°C in M9 medium with 0.4% glucose supplemented with amino acids and vitamins, the same condition as that for the mRNA FISH assay. Figure S6B shows that the growth rate starts to decrease in the presence of ~100 ng/μL novobiocin (Sigma-Aldrich), and keeps dropping as the drug concentration further increases. Our gyrase inhibition condition for mRNA FISH assay was 50 ng/μL novobiocin, under which the cells maintained the same growth rate as that without drug treatment. In addition, there was no cell morphology change upon 50 ng/μL novobiocin treatment for several hours as observed under microscope (data not shown). From the growth rate measurements and cell morphology observations, we conclude that gyrase partial inhibition under our mRNA FISH assay condition did not affect normal physiology of *E. coli* cells, yet allowed us to study the role of gyrase activity in transcriptional bursting.

mRNA Single-Molecule FISH Assay

The BW25993 *E. coli* cells were grown in M9 medium with 0.4% glycerol supplemented with amino acids and vitamins, together with antibiotics and 1 mM IPTG if necessary. The cells were subsequently inoculated 1:500 into the same medium and incubated for ~7 hr at 37°C with 250 rpm shaking till OD_{600nm} reached 0.2~0.3. 50 ng/μL novobiocin was added into the medium and incubated for another 2 hr before harvest. 2 hr was long enough (several cell cycles) to allow all the cells to enter steady state, and thus minimized potential cell-to-cell variation due to different transition kinetics in response to the drug treatment.

The YFP library strains were grown in LB medium with chloramphenicol at 30°C. The cells were subsequently inoculated 1:400 into M9 medium with 0.4% glucose supplemented with amino acids and vitamins and incubated for 11 hr at 30°C with 250 rpm shaking till OD_{600nm} reached 0.2~0.3. 50 ng/μL novobiocin was added and incubated for another 2 hr before harvest.

Upon harvest, the cell culture was mixed with the same volume of ice-cold 2X fixation buffer followed by brief vigorous shaking and 15 min incubation on ice. The 2X fixation buffer consists of 2X RNase-free PBS (Ambion, Life Technologies, Carlsbad, CA) and 6.4% formaldehyde (Electron Microscopy Sciences, Hatfield, PA) in RNase-free water (Ambion). After fixation, the cells were pelleted down by 4700 rpm spinning for 3 min and washed twice in 1 ml ice-cold PBS (Ambion). After the final wash, the cells were first resuspended in ~20 μl PBS and then mixed with 1 ml 70% ethanol for 1 hr incubation at room temperature. After that, the cells were pelleted down by 7000 rpm spinning for 1 min.

The pelleted cells were then washed in 1 ml wash buffer and resuspended in ~20 μl wash buffer. 10 μl of pelleted cells were added to 51.5 μl hybridization mixture described below, and mixed well via tapping and inverting without introducing bubbles. The final hybridization assay was incubated in the dark at 30°C for 9 to 12 hr. After the incubation, the cells were washed twice with 100 μl wash buffer and incubated in the dark at 30°C for 1 hr. The cells were then washed once with 100 μl wash buffer, twice with 100 μl PBS, and finally resuspended in 15 to 20 μl PBS.

In the FISH assay, the hybridization buffer consists of 2X SSC solution (Ambion), 0.2 mg/mL BSA (New England Biolabs), 2 mM RVC (Ribonucleoside Vanadyl Complex; Sigma-Aldrich), 10% dextran sulfate (MW > 500,000; Sigma-Aldrich), 0.1% *E. coli* transfer RNA (Sigma-Aldrich), and 22.1% formamide (Applied Biosystems, Life Technologies). The wash buffer consists of 22.1% formamide and 2X SSC solution in RNase-free water. The FISH probe is a 20-mer oligodeoxynucleotide (Venus495r, 5′ – TCCTCGATG TTGTGGCGGAT – 3′) with a dye molecule Atto 594 covalently linked on the 5′ end through NHS ester reaction followed by RNase-free HPLC purification (custom made by Sigma-Aldrich). A 50 nM FISH probe solution was made by mixing 1 μl 5 μM FISH probe solution, 10 μl 2 mg/mL BSA (New England Biolabs) and 90 μl RNase-free water (Ambion). The hybridization mixture was made by mixing 50 μl hybridization buffer with 1.5 μl 50 nM FISH probe solution.

mRNA FISH Imaging Sample Preparation, Microscopy, and Data analysis

The 35 mm petri dishes (with 14 mm microwell and No. 1.0 coverglass; MatTek, Ashland, MA) were cleaned with the following procedure: 30 min sonication in 1 M potassium hydroxide, 30 min sonication in purified water, blow-dry with nitrogen gas, 10 min cleaning in plasma cleaner, and rinse with purified water. Then the petri dishes were incubated for 1 hr at room temperature with 2 ml 0.033% poly-l-lysine (Sigma-Aldrich) filtered by 0.2 μm syringe filters (Pall Corporation, Northborough, MA). The residual poly-l-lysine solution on the dish was removed completely by rinse with purified water and blow-dry with nitrogen gas. 15 to 20 μl cell culture was applied to the coverglass region of the dish and incubated at room temperature for 1 to 1.5 hr in the dark while covered to prevent evaporation, allowing cell attachment to the poly-l-lysine coated coverslip surface. After the incubation, we gently applied PBS solution to rinse the coverslip surface and wash away the unattached cells. After several times of wash, 2 ml of PBS with 140 mM 2-mercaptoethanol was applied to the dish. By then, the sample was ready for imaging.

An Olympus IX81 microscope with a 100X NA 1.35 phase-contrast objective and an EMCCD (Evolve, Photometrics, Tucson, AZ) was used. For imaging of Atto 594, a 580 nm fiber laser (VFL-P-Series, MPB Communications, Canada) was used. The fluorescence filter set includes an excitation filter (HQ575/50X, Chroma Technology Corp), a dichroic mirror (z594rdc, Chroma), and an emission filter (D635/55M, Chroma). The laser intensity at the focal plane was ~100 W/cm^2. The acquisition time of each image was 1000 ms.

For phase contrast imaging of cell morphology, the same filter set and a build-in lamp in the microscope were used. The acquisition time of each image was 100 ms. Phase contrast and Atto 594 images were acquired for multiple fields of view for each strain. The total number of cells imaged for each condition is ~4000 on average after cell size filtering. Images without laser excitation were recorded as the offset level, and fluorescent images of diluted dye solutions were recorded to correct for slight illumination inhomogeneity across the field of view.

Fluorescent spots corresponding to localized mRNA molecules were identified with a peak-searching algorithm written in Matlab. The algorithm searches for pixels that have both (i) intensity above a predefined threshold and (ii) image curvature above a predefined threshold. The thresholds were determined by eyeballing, such that all the identified peaks correspond to actual fluorescent spots. For each fluorescent spot, the fluorescence intensity above background was integrated over a 5-pixel-by-5-pixel area (corresponding to 800 × 800 nm) surrounding the peak. If more than one peak were identified within the 5-pixel-by-5-pixel area in the same cell, the masks were merged so that each pixel is counted only once. To compensate for gene dosage and cell cycle difference between cells, only a small subset of cells within a certain range of cell size (1.92 μm^2 to 2.30 μm^2) were used for mRNA copy number counting. The calibration of single-molecule fluorescence and the quality control of single-molecule FISH false-positive and false-negative rates were performed as previously described (Taniguchi et al., 2010).

Control Experiments of Gyrase Inhibition and Overexpression Effects on Transcriptional Bursting of Plasmid-Borne Fully Induced lac Operon

For the gyrase inhibition assay, *E. coli* cells containing a plasmid-borne *lac* operon expression module were grown in M9 medium supplemented with 0.4% glycerol plus amino acids and vitamins. 50 ng/μL carbernicillin and 1 mM IPTG were added to maintain the plasmid and fully induce *lac* operon expression, respectively. When the OD_{600nm} value of the cell culture reaches 0.2 to 0.3, 50 ng/μL novobiocin was added into the mixture, which was incubated for 2 hr before cell harvest.

For the gyrase overexpression assay, *E. coli* cells containing a plasmid with *lac* operon expression module and a plasmid with gyrase overexpression module were grown in M9 medium supplemented with 0.4% glycerol, amino acids and vitamins, in the presence of 50 ng/μL carbernicillin, 35 ng/μL kanamycin and 1 mM IPTG. When the OD_{600nm} value of the cell culture reaches 0.2 to 0.3, 0.2% L-arabinose was added into the mixture to induce gyrase overexpression, which was incubated for 2 hr before cell harvest. The mRNA FISH results are shown in Figure S6C.

Derivation of Poisson with Zero Spike Distribution for Cellular mRNA Copy Number

The transcriptional bursting phenomenon can be described by a two-state model:

$$\text{Gene OFF} \underset{\alpha}{\overset{\beta}{\rightleftharpoons}} \text{Gene ON} \xrightarrow{k_1} \text{mRNA} \xrightarrow{\gamma} \varnothing,$$

where k_1 is average transcription rate; γ is mRNA degradation rate constant; α is the transition rate constant from gene "on" to "off" state, limited by gyrase dissociation rate; and β is the transition rate constant from gene "off" to "on" state, limited by gyrase association rate.

Each state of the system can be described by both the gene state and the copy number of mRNA. The transition between different states of the system can be illustrated by the following diagram:

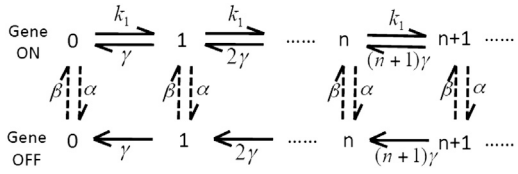

where n represents the state with n copies of mRNA.

The corresponding Chemical Master Equations are

$$\frac{dp_1(n)}{dt} = \beta p_2(n) - \alpha p_1(n) + k_1 p_1(n-1) - k_1 p_1(n) + (n+1)\gamma p_1(n+1) - n\gamma p_1(n);$$

$$\frac{dp_2(n)}{dt} = \alpha p_1(n) - \beta p_2(n) + (n+1)\gamma p_2(n+1) - n\gamma p_2(n),$$

where $p_1(n)$ is the probability of the "on" gene to occupy state n, and $p_2(n)$ is the probability of the "off" gene to occupy state n.

At steady state, we just set the right-hand-side of the Chemical Master Equations to be zero. Then we denote p_1 as the probability for the gene to be "on," and p_2 as the probability for the gene to be "off." We have

$$p_1 + p_2 = \sum_{n=0} (p_1(n) + p_2(n)) = 1,$$

and $\alpha p_1 = \beta p_2$, hence at steady state, we have

$$p_1 = \sum_{n=0} p_1(n) = \frac{\beta}{\alpha+\beta}$$
$$p_2 = \sum_{n=0} p_2(n) = \frac{\alpha}{\alpha+\beta}$$

Assuming α and β are much smaller than k_1 and γ, the cells separate into distinct On and Off populations. For the On population, cellular mRNA copy number follows Poisson distribution, that is

$$p_1(n) \approx p_1 e^{-\frac{k_1}{\gamma}} \frac{\left(\frac{k_1}{\gamma}\right)^n}{n!} = \frac{\beta}{\alpha+\beta} e^{-\frac{k_1}{\gamma}} \frac{\left(\frac{k_1}{\gamma}\right)^n}{n!}$$

For the Off population, cellular mRNA copy number is always zero, i.e.

$$p_2(0) \approx p_2 = \frac{\alpha}{\alpha+\beta}, p_2(n) = 0, n \geq 1$$

The overall distribution is "Poisson with zero spike," i.e.

$$p(0) = p_1(0) + p_2(0) = \frac{\beta}{\alpha+\beta} e^{-\frac{k_1}{\gamma}} + \frac{\alpha}{\alpha+\beta};$$
$$p(n) = p_1(n) + p_2(n) = \frac{\beta}{\alpha+\beta} e^{-\frac{k_1}{\gamma}} \frac{\left(\frac{k_1}{\gamma}\right)^n}{n!}, n \geq 1.$$

For a more rigorous derivation, refer to (Shi and Qian, 2011).

Next we derive the equation of Fano factor based on the "Poisson with zero spike" distribution. The steady-state mean cellular mRNA copy number is

$$\langle n \rangle = \sum_{n=0} n p(n) = \frac{\beta k_1}{(\alpha+\beta)\gamma}.$$

The steady-state variance is

$$\text{var } n = \sum_{n=0} n^2 p(n) - \langle n \rangle^2 = \frac{\beta k_1 \gamma(\alpha+\beta) + \alpha\beta k_1^2}{(\alpha+\beta)^2 \gamma^2}.$$

Therefore the Fano factor is

$$F = \frac{\text{var } n}{\langle n \rangle} = 1 + \frac{\alpha k_1}{(\alpha+\beta)\gamma}.$$

In our two-state model, the average gene "on" state transcription rate k_1 is gene-specific and affected by factors like the global chromosomal supercoiling level via supercoiling-sensitive protein-DNA binding dynamics. As a result, gyrase concentration correlates well with the extent of transcriptional bursting (reflected by β/α), but not necessarily with the average mRNA abundance (k_1/γ) in live *E. coli* cells.

SUPPLEMENTAL REFERENCES

Aitken, C.E., Marshall, R.A., and Puglisi, J.D. (2008). An oxygen scavenging system for improvement of dye stability in single-molecule fluorescence experiments. Biophys. J. *94*, 1826–1835.

Cambray, G., Guimaraes, J.C., Mutalik, V.K., Lam, C., Mai, Q.A., Thimmaiah, T., Carothers, J.M., Arkin, A.P., and Endy, D. (2013). Measurement and modeling of intrinsic transcription terminators. Nucleic Acids Res. *41*, 5139–5148.

Datsenko, K.A., and Wanner, B.L. (2000). One-step inactivation of chromosomal genes in Escherichia coli K-12 using PCR products. Proc. Natl. Acad. Sci. USA *97*, 6640–6645.

Kim, S., Blainey, P.C., Schroeder, C.M., and Xie, X.S. (2007). Multiplexed single-molecule assay for enzymatic activity on flow-stretched DNA. Nat. Methods *4*, 397–399.

Kim, S., Broströmer, E., Xing, D., Jin, J., Chong, S., Ge, H., Wang, S., Gu, C., Yang, L., Gao, Y.Q., et al. (2013). Probing allostery through DNA. Science *339*, 816–819.

Kubitschek, H.E. (1990). Cell volume increase in Escherichia coli after shifts to richer media. J. Bacteriol. *172*, 94–101.

Nagai, T., Ibata, K., Park, E.S., Kubota, M., Mikoshiba, K., and Miyawaki, A. (2002). A variant of yellow fluorescent protein with fast and efficient maturation for cell-biological applications. Nat. Biotechnol. *20*, 87–90.

Pato, M.L., Howe, M.M., and Higgins, N.P. (1990). A DNA gyrase-binding site at the center of the bacteriophage Mu genome is required for efficient replicative transposition. Proc. Natl. Acad. Sci. USA *87*, 8716–8720.

Revyakin, A., Ebright, R.H., and Strick, T.R. (2005). Single-molecule DNA nanomanipulation: improved resolution through use of shorter DNA fragments. Nat. Methods *2*, 127–138.

Schroeder, C.M., Blainey, P.C., Kim, S., and Xie, X.S. (2008). Hydrodynamic Flow-stretching Assay for Single-Molecule Studies of Nucleic Acid-Protein Interactions. In Single-Molecule Techniques: A Laboratory Manual, P.R. Selvin and T. Ha, eds. (Cold Spring Harbor: Cold Spring Harbor Laboratory Press), pp. 461–492.

Shi, P.Z., and Qian, H. (2011). A perturbation analysis of rate theory of self-regulating genes and signaling networks. J. Chem. Phys. *134*, 065104.

Telesnitsky, A., and Chamberlin, M.J. (1989). Terminator-distal sequences determine the in vitro efficiency of the early terminators of bacteriophages T3 and T7. Biochemistry *28*, 5210–5218.

Tycon, M.A., Dial, C.F., Faison, K., Melvin, W., and Fecko, C.J. (2012). Quantification of dye-mediated photodamage during single-molecule DNA imaging. Anal. Biochem. *426*, 13–21.

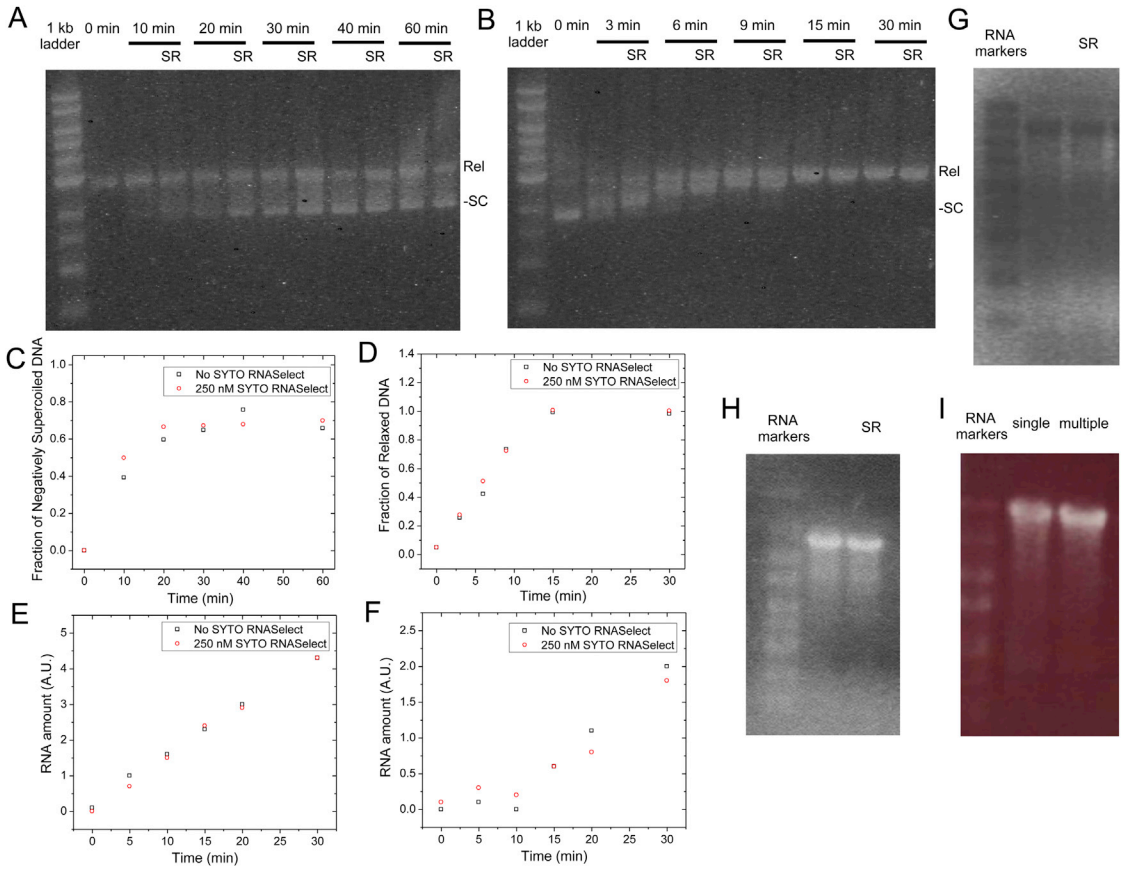

Figure S1. Enzyme Activities under the Condition of the In Vitro Single-Molecule Transcription Assay, Related to Figures 2, 3, 4, and 5

(A) Time dependence of negative supercoiling of relaxed pUC19 plasmid by *E. coli* gyrase in the absence or presence of 250 nM SYTO RNASelect (SR). The position of relaxed pUC19 (Rel) and its most supercoiled topoisomer (-SC) are marked.

(B) Time dependence of relaxation of negatively supercoiled pUC19 plasmid by *E. coli* Topo I in the absence or presence of SR.

(C) The fraction of negatively supercoiled pUC19 in the total amount of pUC19 after gyrase treatment for different time. The amounts of pUC19 were measured from the intensity of bands in (A).

(D) The fraction of relaxed pUC19 in the total amount of pUC19 after Topo I treatment for different time. The amounts of pUC19 were measured from the intensity of bands in (B).

(E) The amount of mRNA generated by in vitro T7 transcription for different time in the absence or presence of SR. The amounts of mRNA were measured by Qubit RNA assay.

(F) The amount of mRNA generated by in vitro *E. coli* transcription for different time in the absence or presence of SR. (C) to (F) demonstrated that the enzymes are ~100% functional in the presence SR, as their reaction rates were not affected.

(G) *E. coli* transcription in the presence of SR produced full-length transcripts. From left to right: 0.2-10 kb RNA markers (lane 1, from Sigma-Aldrich), 5.3 kb *lac* operon mRNA produced by *E. coli* transcription in the absence (lane 2), or presence of SR (lane 3).

(H) T7 transcription in the presence of SR produced full-length transcripts. From left to right: 0.2-10 kb RNA markers (lane 1), 5.3 kb *lac* operon mRNA produced by T7 transcription in the absence (lane 2), or presence of SR (lane 3).

(I) T7 transcription on linear templates anchored on beads produced full-length transcripts. From left to right: 0.2-10 kb RNA markers (lane 1), 12 kb *nuoB-N* mRNA produced by T7 transcription using templates with single (lane 2) or multiple (lane 3) biotin-streptavidin linkages to the bead surface.

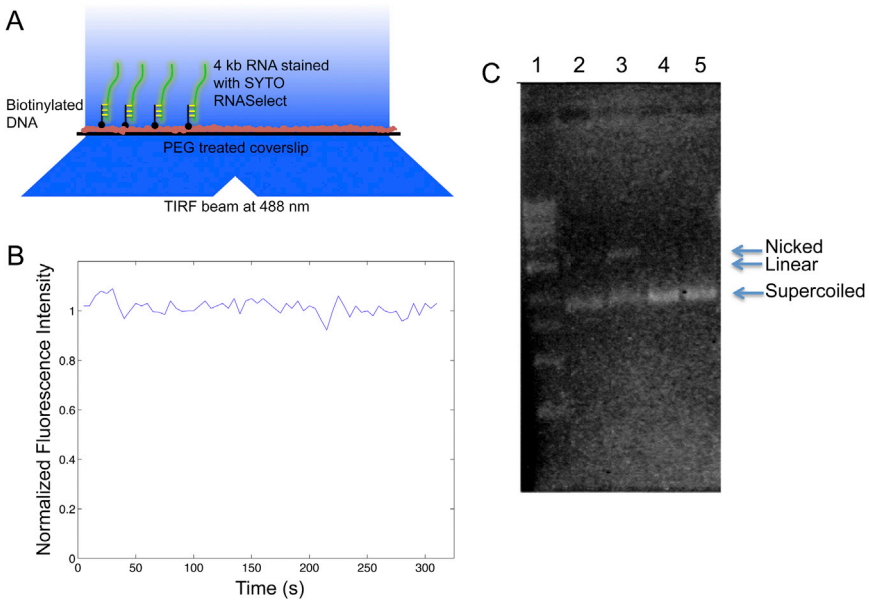

Figure S2. Tests for RNA Photobleaching and DNA Photocleavage in the In Vitro Single-Molecule Transcription Assay, Related to Figures 2, 3, 4, and 5

(A) Schematic representation of the experimental arrangement for the RNA photobleaching assay (not drawn to scale).

(B) Total fluorescence intensity versus time trajectory from 67 individual RNA molecules immobilized on the surface. The intensity barely changed over time, indicating negligible photobleaching.

(C) Minimal DNA photocleavage occurred in the presence of 250 nM SYTO RNASelect during the time for transcription initiation rate measurement. From left to right: 1 kb DNA ladder (lane 1), supercoiled pUC19 DNA after 30 min of 488 nm laser illumination at 0.22 W/cm^2 (lane 2) or 7.3 W/cm^2 (lane 3) in the presence of 250 nM SYTO RNASelect, supercoiled pUC19 DNA without any treatment (lane 4), or after 30 min of incubation with 250 nM SYTO RNASelect in dark (lane 5). While some pUC19 DNA became nicked after high-power illumination, barely any nick or double-stranded breaks were generated on the DNA after laser illumination at the same power level in the in vitro single-molecule assay.

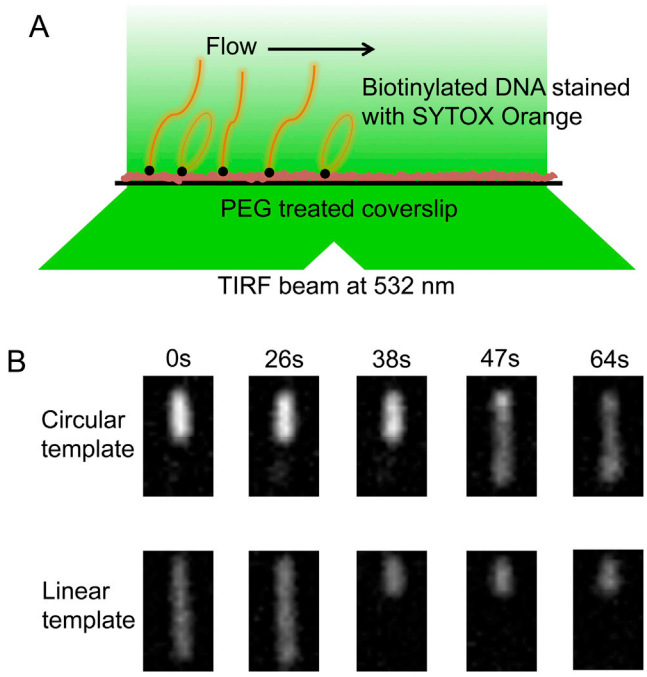

Figure S3. DNA Staining Assay for Identifying Circular DNA Templates, Related to Figures 4 and 5

(A) Schematic representation of the experimental arrangement for the DNA staining assay (not drawn to scale).

(B) Flow-stretched circular and linear DNAs behaved differently when they underwent double-strand photocleavage in the presence of SYTOX Orange. Because double-strand breaks occurred one at a time, a circular DNA appeared to "grow" first because it was cut to become two linear DNAs, one long and one short, which were shortened subsequently. However, a linear DNA could only be cut shorter and shorter.

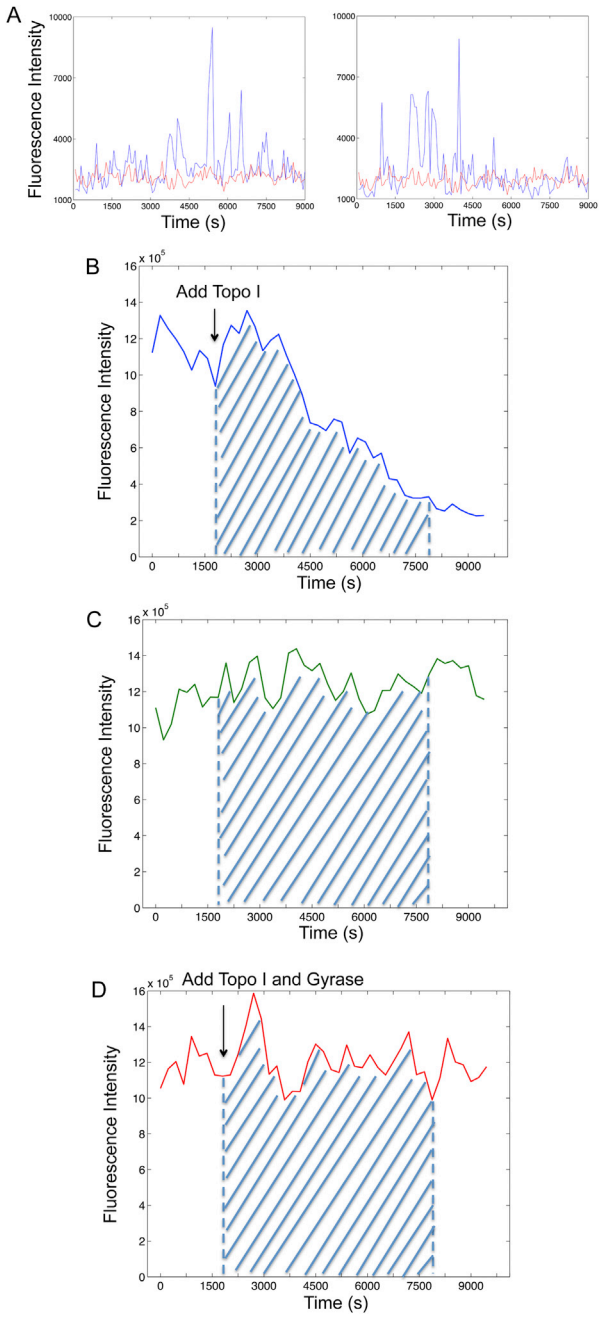

Figure S4. Calculation for the Number of Transcripts Leading to Inhibition of Transcription Initiation through Positive Supercoiling Accumulation, Related to Figure 4

(A) Two fluorescence intensity trajectories from individual circular DNA templates in the in vitro single-molecule transcription assay with T7 RNApol concentration of 2.2 nM. A point was taken every 75 s.

(B) Total intensity versus time from 160 circular templates during in vitro T7 transcription in the presence of 41 nM Topo I, same as Figure 4E. The shaded region corresponds to the total number of transcripts generated by the 160 templates between the moments of Topo I addition and transcription initiation inhibition (~20% of initial value), which covers a period of 5850 s.

(C) Total intensity versus time from 160 circular templates during in vitro T7 transcription in the absence of topoisomerases, same as Figure 4A. The shaded region corresponds to the total number of transcripts generated by the 160 templates during 5850 s.

(D) Total intensity versus time from 160 circular templates during in vitro transcription in the presence of 41 nM Topo I and 0.1 μM gyrase, same as Figure 4C. The shaded region corresponds to the total number of transcripts generated by the 160 templates during 5850 s.

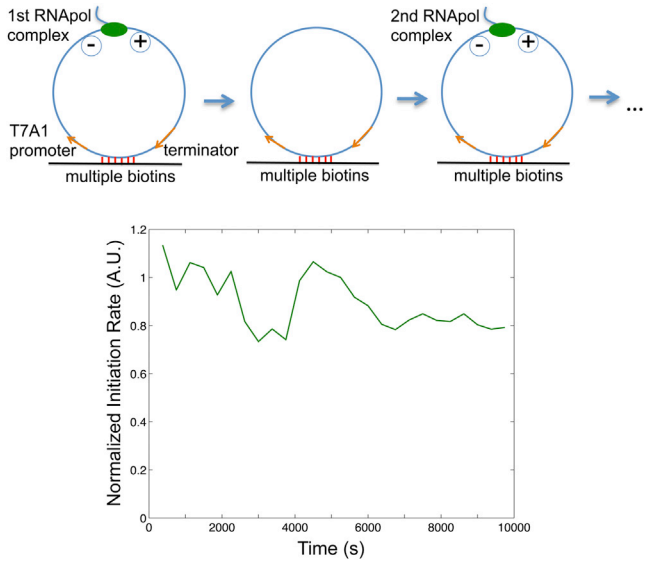

Figure S5. Time Dependence of the Initiation Rate of *E. coli* Transcription on the Circular Templates in the Absence of Topoisomerases, Related to Figure 4

Upper: Schematic of transcription on the circular template in the absence of topoisomerases. Positive and negative supercoiling are generated on the template as RNApol elongates, which annihilate each other after RNApol completes transcription and dissociates from the template. Bottom: *E. coli* transcription initiation rate was constant over time because of repetitive annihilation of supercoiling. The intensity averaged from 137 circular templates at each time point was normalized to that from 256 linear templates.

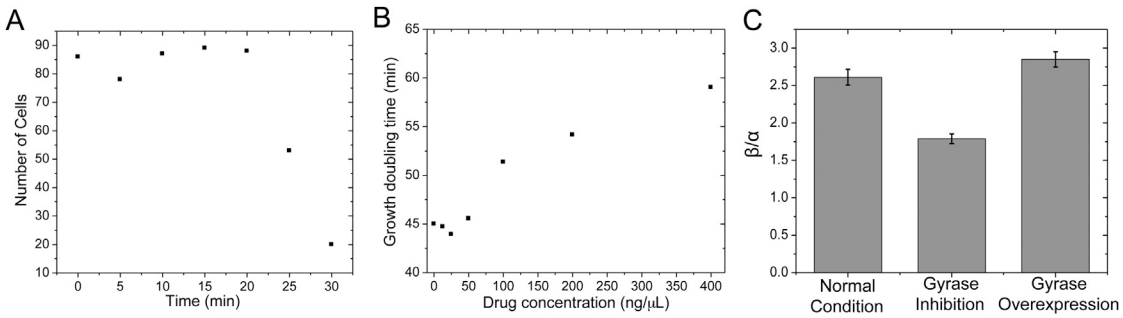

Figure S6. Killing Curve and Growth Rate Measurement upon Gyrase Inhibition and On/Off Duty Cycle Ratio, β/α, for Fully Induced Plasmid-Borne *lac* Operon, Related to Figures 6 and 7

(A) The number of *E. coli* cells (A.U.) versus time after 10 ng/μL norfloxacin treatment. The number of cells was measured by serial dilution, LB plating and colony counting after overnight incubation at 37°C.

(B) Cell growth doubling time versus various concentrations of novobiocin in M9 medium supplemented with 0.4% glucose, amino acids and vitamins at 37°C shaker. The doubling time was measured by the initial OD_{600nm} value, the final OD_{600nm} value and the time interval in between.

(C) β/α decreased upon gyrase inhibition and increased upon gyrase overexpression. The error bars are bootstrapped confidence intervals. Under the same conditions, β/α of the plasmid-borne system was always higher than its chromosomal counterpart (Figure 7D).

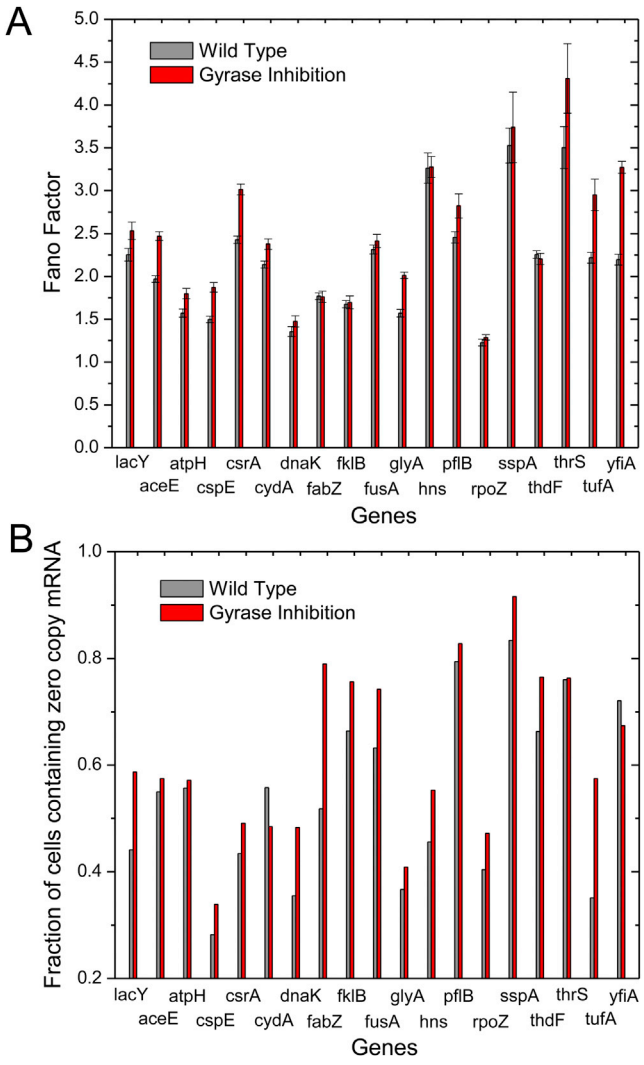

Figure S7. Fano Factors of Steady-State Intracellular mRNA Copy Number Distribution and the Fraction of Cells Containing Zero Copy mRNA for Fully Induced *lac* Operon and 18 Other Highly Transcribed *E. coli* Genes, Related to Figure 7

The error bars are bootstrapped confidence intervals.